www.sciencemag.org/content/355/6326/739/suppl/DC1

Supplementary Materials for

Treadmilling by FtsZ filaments drives peptidoglycan synthesis and bacterial cell division

Alexandre W. Bisson-Filho,* Yen-Pang Hsu,* Georgia R. Squyres,* Erkin Kuru,,* Fabai Wu, Calum Jukes, Sun, Cees Dekker,†‡ Seamus Holden,†‡ Michael S. VanNieuwenhze,†‡ Yves V. Brun,†‡ Ethan C. Garner†‡

*These authors contributed equally to this work.

†These authors contributed equally to this work.

‡Corresponding author. Email: egarner@g.harvard.edu (E.C.G.); mvannieu@indiana.edu (M.S.V.); ybrun@indiana.edu (Y.V.B.); seamus.holden@newcastle.ac.uk (S.H.); c.dekker@tudelft.nl (C.D.)

Published 17 February 2017, *Science* **355**, 739 (2017)
DOI: 10.1126/science.aak9973

This PDF file includes

Other Supplementary Material for this manuscript includes the following:
(available at www.sciencemag.org/content/355/6326/739/suppl/DC1)

Movies S1 to S10 also available at http://garnerlab.fas.harvard.edu/FtsZ/
Code available at https://bitbucket.org/garnerlab/bisson-2016

Author Contributions

This work represents the combined research directions of 3 groups (EG, YB/MV, SH/CD). FDAA labeling and 3D-SIM by YH and EK**.** Strains constructed by AB, GS, and CJ. Confocal and TIRF imaging by AB and GS. Microholes designed by SH and CD, fabricated by FW, and imaged by SH and CJ. Programming by GS, SH and YS. All authors designed experiments and wrote the paper.

Materials and Methods

Culture growth. All *B. subtilis* strains were prepared for experimentation as described below, unless otherwise noted. Strains were streaked from -80°C freezer stocks onto LB agar plates, and grown overnight at 37°C. Single colonies were transferred to liquid cultures in CH medium or PHMM Media - used to grow cells that were not chained (equal parts of CH and $S7_{50}$, with final concentrations of 1 mM glutamate, 0.5% glucose and 100 mM $MgCl_2$). Cells were placed on a roller drum for agitation and grown at 37°C. After cultures reached OD_{600} < 0.5, serial dilutions were grown for one more round until OD_{600} ~ 0.5. Alternatively, cultures were grown overnight at 25°C and then these starter cultures were diluted into the same media and grown at 37°C. bGS28 and bGS31 were grown with 50-100 μM IPTG to induce Pbp2B expression.

Western blots. Wild type (PY79), mNeonGreen-FtsZ (bAB185), FtsA-mNeonGreen (bAB167) and mNeonGreen-Pbp2B (ME7) were grown in 3 mL LB at 37°C until they reached OD_{600} ~ 0.5, then diluted 10-fold to OD_{600} ~ 0.05 and grown again until OD_{600} ~ 0.5. Cultures were centrifuged at 13,000 rpm for 2 minutes, washed once with lysis buffer (20 mM Tris, pH 7.5, 100 mM NaCl, 10 mM EDTA, 1 mM PMSF) and pellets stored at -80°C overnight. Pellets were resuspended in 50 μl of lysis buffer with 10 μg/ml DNAse I, 100 μg/ml RNAse A and 10 mg/ml of lysozyme and incubated at 37°C for 20 minutes. Small aliquots were used to determine total protein mass (Pierce BCA Protein Assay Kit). 10, 25 and 50 μg of the lysates were then separated by SDS PAGE in 10% Bis-Tris gels, and blotted to 0.2 μm nitrocellulose membranes (Bio-Rad). The One-Hour Western Chemiluminescence Detection System kit (GenScript) was used coupled with primary antibiodies against FtsZ (anti-rabbit), FtsA (anti-mice) and Pbp2B (anti-rabbit). Antibodies were a gift from Jeff Errington, Frederico Gueiros Filho and Richard Daniel, respectively. Images were taken by a CCD camera coupled to the Chemilmager 5500 System (Alpha Innotech).

Fluorescent D-amino acids synthesis. HADA (7-hydroxycoumarin-3-carboxylic acid-D-alanine), BADA (BODIPY FL-D-alanine) and TADA (TAMRA-D-alanine) were synthesized as reported previously (*5, 25*). 7-hydroxycoumarin-3-carboxylic acid (for HADA, 1.45 mmole) or BODIPY FL (for BADA, 1.45 mmole) was added to a 100 ml, flame-dried round flask containing 14.5 ml anhydrous DMF and a stir bar. After adding 1.45 mmole carbonyldiimidazole to the flask, the reaction was stirred at room temperature (RT) for 2 hours, following by directly adding 1.45 mmole N^{α}-Boc-D-2,3-diaminopropionic acid. The reaction was stirred overnight under argon atmosphere. The solvent was removed *in vacuo* and the product was extracted with EtOAc and 0.33N HCl/H_2O, and treated with trifluoroacetic acid and dichloromethane in 1:1 ratio for 30 min with stirring at RT. The final product was purified via reverse-phase HPLC with 10-90% MeCN/H_2O gradient. For TADA synthesis, N^{α}-Boc-D-2,3-diaminopropionic acid (1.45 mmole),

5-(and 6-) carboxytetramethylrhodamine succinimidyl ester (1.45 mmole), and diisopropylethylamine (200 µl) were added in one portion to a 100 ml round flask containing 14.5 ml anhydrous DMF. The reaction was stirred under argon overnight at RT. The product was de-protected and purified as described above.

Fluorescent D-amino acids labeling. FDAA stock solutions were prepared in DMSO (Sigma-Aldrich ReagentPlus >99.5%) at a concentration of 100 mM and stored at -20°C before use. The labeling conditions, including incubation interval and color order, are indicated in each FDAA figure and summarized in Table S1.

FDAA-I. For the sequential labeling in Fig. 1A, exponential phase cells (PY79) at OD_{600} ~ 0.5 were diluted with PHMM containing 1 mM HADA to OD_{600} ~ 0.1, and then grown for 1 hour at 37°C. Cells were washed twice with fresh PHMM (37°C), and centrifuged between washes (6,000 g for 1 minute at room temperature). For the second labeling, the cell pellets were resuspended in pre-warmed PHMM containing 1 mM BADA for 5 minutes. After this, cells were washed twice, and labeled a third time by resuspending in pre-warmed PHMM containing 2 mM TADA for 30 seconds. Cells were then immediately treated with 70% ice-cold ethanol, and incubated on ice for 1 hour. Ethanol-fixed cells were collected via centrifugation (10,000 g for 5 minutes at 4°C), washed twice with 4°C 1 x Phosphate Buffered Saline (PBS, pH 7.4), resuspended in PBS, and stored on ice before imaging.

FDAA-II. For the short-pulse labeling in Fig. 1B, 1E and S1A, cells (PY79) were first labeled with HADA (0.5mM, 60-90 minutes) and washed as described in **FDAA-I**. Cells were then transferred to a syringe filter (Acrodisc, 0.2 µm HT Tuffryn, 25 mm), and pre-warmed, fresh PHMM media (10 ml) was added to wash out excess dye. The cells were then treated sequentially with PHMM-FDAA media (2 mM BADA or TADA in 1 ml media for 15 sec), PHMM media (for washing), and PHMM-FDAA/Bocillin media (2 mM FDAA or 50 µg/ml Bocillin in 1 ml media for 15 sec) to label the cells. After washing with 10 ml PBS, cells were collected by back-sucking fixation reagent through the filter into the syringe. For Fig. 1B and S1A, 70% ethanol was used for fixation as described in **FDAA-I**. For Fig. 1E, to preserve the Bocillin signal, cells were fixed in 4% para-formaldehyde for 30 minutes at room temperature. Cells were collected by centrifugation (10,000 g for 5 minutes at 4°C), washed, and stored in PBS on ice before imaging.

FDAA-III. For time-course labeling in Fig. 1D, cells (PY79) were first labeled with HADA (1 mM, 60 minutes) as described above. The collected cells were resuspended in pre-warmed PHMM containing TADA (2 mM in 0.3 ml) and incubated for 15-120 seconds in a 37°C water bath. The cells were then fixed with 70% ethanol as described above. Labeling in Fig. S1B-C was performed similarly, using the FDAAs in a different order (see Table S1).

FDAA-IV. For FDAA labeling with antibiotic treatments in Fig. S2D, cells (PY79) were first labeled with HADA (1 mM, 60 minutes) as described above. Cell pellets were then resuspended in pre-warmed PHMM containing antibiotics (4 µg/ml Vancomycin or 50 µg/ml Penicillin G) and incubated for 3 minutes in a 37°C water bath. Next, TADA stock solution was added directly to the cells to a final concentration of 2 mM. After a 2 minute incubation, cells were fixed with 70% ethanol and collected as described above.

FDAA-V. For FDAA labeling with Pbp2B depletions in Fig. S2D, exponential phase cells (bGS3) were diluted with PHMM containing 1 mM HADA to OD_{600} ~ 0.1, and grown for 3 hours at 37°C without IPTG to deplete Pbp2B. Following two washing steps with fresh PHMM (37°C), cell pellets were resuspended in pre-warmed PHMM containing 2 mM TADA and incubated for 2 minutes. The cells were fixed with 4% para-formaldehyde as described above.

FDAA-VI. For FDAA labeling with FtsZ(D213A) expression in Fig. 4A, exponential phase cells (bAB217) were grown in PHMM containing 100 μM IPTG for 60 min, treated with TADA (2mM, 3 min), washed twice with pre-warmed PHMM, and then labeled with HADA (2 mM, 3 min). The cells were washed and then fixed with 4% para-formaldehyde as described above. For Fig. 4B, exponential phase cells (bAB217) were diluted with PHMM containing 1 mM HADA to OD_{600} ~ 0.1. After 30 minutes of growth at 37°C, IPTG was added to the culture to a final concentration of 20 μM, and incubated for another hour. Following two washing steps with fresh PHMM (37°C) containing IPTG, cells were resuspended in fresh PHMM containing 2 mM TADA and IPTG, then incubated for 1 minute. The cells were then fixed with 70% ethanol and washed.

FDAA-VII. For FDAA labeling with PC190723 treatment in Fig. 4B, exponential phase cells (PY79) were diluted with PHMM containing 1 mM HADA to OD_{600} ~ 0.05. After a 90-minute growth at 37°C, PC190723 (10 mg/ml, DMSO stock) was added to the culture to a final concentration of 1 μg/ml, and incubated for another 10 min. Following two washing steps with fresh PHMM (37°C) containing PC190723, cells were resuspended in fresh PHMM containing 2 mM TADA and PC190723, then incubated for 1 minute. The cells were then fixed with 70% ethanol as described above. Labeling in Fig. S6A was performed similarly, using 10 μg/ml PC190723 and 2 min of TADA labeling.

FDAA-VIII. For FDAA labeling with MciZ expression in Fig. 4B, exponential phase cells (strain AH93) were diluted with PHMM containing 1 mM HADA to OD_{600} ~ 0.05. After a 90-minute incubation at 37°C, 50 mM xylose was added to the culture, and the cells were incubated for 5 minutes. Following two washing steps with fresh PHMM (37°C) containing xylose, cells were resuspended in fresh PHMM containing 2 mM TADA and 50 mM xylose, then incubated for 30 seconds. The cells were fixed with 70% ethanol as described above.

HaloTag labeling with Halo-TMR and JF- dyes. For the Fig. 2D, full labeling of FtsA-HaloTag(SW) (see strain construction for details) was obtained by incubating strain bAB229 with 500 nM HaloTag-JF549 ligand for 15 min. For Fig. 2F and 3E, Pbp2B single molecules were obtained by incubating bGS31 (*HaloTag-pbp2B*) with 40-100 pM of HaloTag-JF549 ligand for 15 min; cells were washed once in fresh media to remove free dye before imaging. For Fig. 3C, FtsA single molecules were obtained by incubating bAB213 (*ftsA-HaloTag(SW)*) with 250 pM of HaloTag-JF646 ligand for 15 min. HaloTag ligands were a gift of Luke Lavis (*14*).

Depletions in liquid culture. For the Pbp2B depletions shown in Fig. 3B and Movie S5, bGS31 cells (*ftsZ::mNeonGreen-ftsZ*, *erm-Phyperspank-HaloTag-pbp2B*) were grown in liquid culture with 10 μM IPTG until OD_{600} ~ 0.5, the inducer was washed out, and then cells were shifted to media lacking IPTG. Before imaging mNeonGreen-FtsZ, cells were observed under microscope every 30 minutes until no divisions were observed to ensure Pbp2B depletion.

Expression of *ftsAZ* constructs. For all experiments in which the expression of a second copy of tagged FtsA and/or FtsZ was required, fusions were made in a way to maintain the operon structure to avoid perturbations on the FtsA/FtsZ ratio (*26, 27*). As shown in Fig. S3F, increased levels of either FtsA or FtsZ can impair cell division, while high levels of FtsAZ did not present an observable phenotype.

Perturbations in CellASIC microfluidic system. To observe the effects of MciZ (Fig. 3F, Movie S7B) and PC190723 (Fig. 3E, Movie S8A) on FtsAZ motion, we used the microfluidic CellASIC system from EMD Millipore with B04A plates. Cells in optimal growth conditions (as described in the culture growth section) were loaded into the device and equilibrated for 1 hour in CH media at a flow of 3 PSI. Afterward, based on the observation that exogenous MciZ is capable of penetrating cells and inhibiting Z ring assembly (*28*), cells were flowed with 1 μM of synthetic MciZ peptide or 10 μM of PC190723 at 5 PSI and imaged by TIRF microscopy. Pulses and washes were performed as needed and described in each figure legend. Synthetic MciZ peptide and PC190723 drug were purchased from PSL Peptide Specialty Laboratories GmbH and EMD Millipore, respectively.

Antibiotic treatments. For the effect of different antibiotics on FtsAZ motion (Fig. 3A and Movie S4), cells were grown in liquid as described above and placed under agarose pads (500 μl of media with 2% agarose). After FtsAZ motion was confirmed by TIRF microscopy, 3 μl of the antibiotic was added on top of the pad, followed by 5 minutes of incubation. Time lapses were then acquired from different fields of view. Antibiotic concentrations were as follows: 10 mg/μl Ampicillin (blocks transpeptidation); 10 mg/μl Penicillin G (blocks transpeptidation); 50 mg/μl Vancomycin (blocks transpeptidation and transglycosylation); 100 mg/μl Fosfomycin (blocks PG precursor synthesis); 100 mg/μl Cephalexin (blocks transpeptidation). To confirm the effect of each specific treatment, we conducted separate experiments where we incubated liquid cultures with each antibiotic (at a final concentration of 10 μg/μl) for 5 minutes, followed by imaging.

Correlation between FtsAZ motion and cytokinesis rates. For the effects of different genetic backgrounds and overexpression of a number of components on FtsAZ motion and cytokinesis rates (shown in Fig. 4C, Table S4, Movie S10), cells were grown in liquid as described above and placed under agarose pads. Where inducible promoters were used, the appropriate IPTG concentration (0, 1, 5, 7.5, 10 and 100 μM) was mixed into to the pad. The exception to this protocol was the experiments with MciZ-expressing cells. Because very low concentrations of MciZ can quickly block cell division (*20, 29*), MciZ was only induced after cells were under the agarose pad, by addition of 5 μl of a 3M xylose solution on top of the 500 μL pad (as with the antibiotic perturbations described above). Each condition was imaged on a spinning disk confocal (for Pbp2B ring constriction) and on a TIRF microscope (for FtsAZ filament dynamics). The strains, conditions, and measurements for each experiment are shown in Table S4. mNeonGreen-Pbp2B was used as a reporter of cytokinesis, and the constriction times were measured by manual kymographs. These measurements were then validated by automated analysis. **Manual tracking:** For each condition, 100 random rings were cropped, and kymographs were drawn along the ring axis using Fiji. From these kymographs we determined when ring constriction initiated by using the time point where the slope of the edge of the signal switched from being vertical to angled (top dotted line). The disappearance of Pbp2B was used to indicate the end constriction period (assayed by the last bright pixel in the kymograph). The difference in these two time points was taken as

the constriction interval for each ring. **Automated analysis**: To independently validate these manual measurements, we applied an automated analysis of the cytokinesis time. We exploited the fact that mNeonGreen-Pbp2B rings get brighter up until they begin constriction to set a threshold for each image based on the average of intensity of 100 constricting rings. We then applied this threshold to entire fields of cells. We then tracked these thresholded rings with the TrackMate plugin to determine each ring's lifetime (*30*). We set a lifetime cutoff between 5-30 minutes, to exclude rings that that were already at late stages of constriction, or anomalous constrictions.

Microholes nanofabrication. Microholes are patterned through electron-beam lithography as described previously (*31*) and etched through a reactive-ion etching (*32*). Briefly, a silicon wafer was spin-coated with resist NEB-22 (Sumitomo Chemical). Predesigned features were patterned through Leica EBPG 5000+ with a beam step size of 20 nm. The exposed resist was removed by solvent Microposit MF-322 solution and the exposed wafer surface was etched using an AMS Bosch Etcher. The remaining resist was removed using oxygen plasma.

Culture growth for vertical microhole immobilization. *B. subtilis* strains to be imaged by vertical microhole immobilization were streaked from -80°C freezer stocks onto LB agar plates, grown at 30°C in Time Lapse Medium (TLM) (*33*) overnight, re-diluted in pre-warmed Chemically Defined Medium (CDM) (*33*) and grown at 30°C to OD_{600} ~ 0.4 before being immobilized in agarose microholes (see below).

Imaging – slide preparation. Coverslips were sonicated in 2% Hellmanex (Hellma GmbH&Co, Milllheim, FRG) for 30 minutes, followed by multiple washes with deionized water, then sonicated with 1 M KOH for 30 minutes, followed by multiple washes with water. Coverslips were washed twice with 100% ethanol, and then sonicated for 30 minutes in 100% ethanol, followed by one more wash in 100% ethanol. They were stored in ethanol and dried before use.

Imaging – Pbp2B and FtsZ ring constriction rates. Images were collected on a Nikon TI spinning disk confocal microscope with Yokogawa CSU-10 spinning disk and a Hamamatsu ImagEM (EM-CCD) camera (effective pixel size 110 nm), and Nikon 100X NA 1.45 TIRF objective. Illumination was accomplished using fiber coupled Spectral lasers, using a 488 laser for imaging of mNeonGreen, and a 494 nm laser for imaging of FM5-95. For the experiments following ring constriction, time lapses were acquired with 1 minute intervals for 2 hours with exposure times of 50-150 milliseconds.

Imaging – FtsAZ and Pbp2B dynamics by TIRFm. Images were collected on a Nikon TI microscope equipped with a 6.5 μm pixel CMOS camera and an EMCCD camera, together with a Nikon 60X NA 1.40 and a Nikon 100X NA 1.45 objective set. Exposure times varied between 0.1 and 3 seconds, as indicated. Illumination was accomplished using a fiber coupled Agilent launch with for 405 nm, 488 nm (imaging of mNeonGreen and msfGFP fluorescent proteins), 561 nm (imaging of JF549 dye) and 647 nm (imaging of JF646 dye).

Imaging – 3D-SIM of FDAA labeling. 3D-SIM images were collected on DeltaVision OMX system (Applied Precision Inc, Issaquah, USA) equipped with 1.4 NA Olympus 100X oil objective, laser source (405, 488, 561 and 642 nm) and four photometrics Cascade II EM-CCD cameras. 24X50 mm coverslips (# 1.5) were used as imaging support for the inverted system. Cell

samples were loaded on the coverslips, followed by laying an 8X8 mm wide, 2 mm thick PBS-agar pad on top of the cells. The coverslip-pad combination was placed onto the OMX microscope in a sample stage plate with the pad facing upwards. 3D-SIM imaging was controlled with the DV-OMX software. FDAA signal was captured by using: 1) for HADA, 405 nm laser with 419-465 nm emission filter; 2) for BADA, 488 nm laser with 500-550 nm filter; and 3) for TADA, 561 nm laser with 609-654 nm filter. The z-axis scanning depth ranged from 2.4 to 3 μm. The immersion oil was optimized for each experiment with a range from 1.514 to 1.518.

Imaging – agarose microhole sample preparation Agarose microholes were created by pouring molten 6% agarose onto a silicon micropillar array (Fig. S4). Patterned agarose was transferred into a Geneframe (Thermo Scientific AB-0577) mounted on a glass slide. The regions either side of the microholes were cut away, leaving a thin strip of agarose in the center of the Geneframe, to ensure sufficient oxygen. Cells at OD_{600}~0.4 were concentrated 100x by centrifugation. 4 μL of sample was then loaded onto the agarose pad and a cover slip was placed on top.

Imaging – FtsZ dynamics in agarose microholes. FtsZ dynamics were imaged by near-TIRF illumination on a Nikon N-STORM microscope equipped with an NA 1.49 Nikon 100x TIRF objective, laser source (488 nm), additional 2.5x magnification optics and a 16 μm pixel Andor iXon DU897 EMCCD, giving a final pixel size at the image plane of 64 nm. Exposure times were 1 s and images were taken at 1 s intervals. The temperature at the sample was 30.0°C.

Image processing. All image processing unless otherwise specified was performed in Fiji (*34*). Images used for particle tracking were unaltered, except for trimming two pixels from the edges of some videos to remove edge artifacts detected by the tracking software. Images were cropped, contrast adjusted, rotated and scaled (no interpolation) for figures. SIM images were reconstructed using softWoRx and the quality was confirmed by SIMcheck (*35*). 3D projections were obtained with the Volume Viewer function of softWoRx with 25 stacks. The image of the 13th stack (90°-rotated) was used for data analysis.

Data analysis – kymographs. Kymographs were generated by the Fiji *kymograph* plugin with a line width of 3 (for FtsA and FtsZ) or 5 (for Pbp2B). For kymograph-based velocity measurements, velocities were quantitated by measuring the length of fluorescent trajectories in pixels and converting to nm and sec, respectively. For constriction times, kymographs of each condition were plotted and the intervals converted from the length of line segments in pixels: see "Correlation between FtsAZ motion and cytokinesis rates" above for details.

Data analysis – particle tracking. For particle tracking, tracks were generated using the TrackMate plugin in Fiji (*30*). Particles were detected with the Laplacian of Gaussians (LoG) detector, with a 400 nm blob diameter. Tracks were generated using the Linear motion LAP Tracker, with a 100 nm search radius and no frame gaps allowed. Tracks were then exported into MATLAB for further processing. For the characterization of FtsZ and A single molecules, we included all tracks containing 5 or more frames, since frames 4 and under cannot be fit by the velocity calculating algorithm; no additional filtering was done. For the characterization of FtsZ, FtsA and Pbp2B velocity, we applied additional filters to select for tracks with quantifiable directional motion. Using a custom script, tracks were filtered to select for directionally-moving tracks and exclude background, erroneous assignments, and, in the case of Pbp2B, rapidly

diffusing molecules outside of the Z ring. Tracks shorter than 10 seconds or longer than 25 seconds were excluded, as were tracks whose start to endpoint displacement was less than 50 nm. For each track, the velocity, the diffusion coefficient, and the scaling exponent α were calculated as described previously (*15*). Briefly, mean squared displacement vs time delay (MSD vs *t*) was calculated for each track. Linear fits were made to log(MSD(*t*)) vs log(*t*); α is the slope of this fit. To ensure the quality of the tracks, only tracks with $r^2 > 0.95$ for this linear fit were included in the data set. Velocity and diffusion coefficient were then calculated by fitting $MSD(t) = 4D(t) + (Vt)^2$ using nonlinear least-squares fitting (*15*).

Data analysis – photobleaching traces. Images for photobleaching analysis were collected with 200 ms exposures, acquiring continuously (5 frames/second) to ensure sufficient time resolution. Representative particles were chosen manually. Using Fiji, intensity traces were generated from a 5x5 pixel region that was centered on the particle. To reduce noise, intensity traces were then filtered using a median intensity filter with a 4 second time window. The filtered trajectories were normalized to their minimum and maximum values: this was necessary because, particularly in TIRF, illumination intensity is non-uniform across the field of view. For plotting, intensity traces were aligned such that time t=0 corresponds to the frame in which the particle appears.

Data analysis – vertical microhole imaging. Images were corrected for translational drift using the Fiji *StackReg* plugin. Kymographs were automatically calculated along the circumference of individual Z rings using a custom MATLAB script. The best fitting circle for each Z ring was identified by least squares fitting, and the intensity around the circumference of the ring calculated with sub-pixel precision by bicubic interpolation. FtsZ velocities were calculated as per the kymographs above. Mean filament speed in Fig. S4E measured by Gaussian fitting.

Data analysis – plots. Plots were generated using Prism and MATLAB. Violin plots were generated in MATLAB using the violin.m function (*36*). Horizontal error bars were added to Fig. 4C using the ploterr.m function (*37*). In plots, ns and * is used to indicate the result of an unpaired two-sample t-test: ns $p \geq 0.05$, *$p < 0.05$, **$p < 0.01$, ***$p < 0.001$, ****$p < 0.0001$.

Data analysis – 3D-SIM. To confirm that 3D-SIM images could be used for intensity quantitation, we demonstrated that intensity of Tetraspeck beads scaled linearly with exposure time after reconstruction (Fig. S2A). For quantitative analyses, septal PG images were collected by cropping the division site of the cells (~1.5 x 0.5 μm) using softWoRx software (Applied Precision, Issaquah, WA). Long-pulse labeling of FDAA (usually HADA) was used to identify the division sites and cell division state. Only the cells having a clear division site but not yet a complete septum were collected and analyzed. To quantify total intensity, we summed the intensity of 3D projections of Z rings. To quantify area labeled, we counted the number of pixels in the image that were above a set intensity threshold. Because the choice of threshold was arbitrary, where this metric was used, we demonstrated that the observed trends were independent of threshold choice (Fig. S2B). For total area labeled, we summed all the labeled pixels in the image; this represents total amount of FDAA labeling. For average feature area, we counted the number of pixels in each discrete labeled region of FDAA; this indicates the amount of FDAA labeling per spot. For the time course data in Fig. 1D and S2B-C, images from the longer labeling times (60, 90, and 120 seconds) were acquired with half the exposure time of the shorter labeling times to avoid saturating

intensities. To compare these time points, we corrected the intensity for the later time points by multiplying their values by 2; we confirm that intensity scales linearly with exposure time in Fig. S2A. Violin plots were generated in MATLAB using the violin.m function (*36*). To compute the correlation between images, we first background subtracted each image in Fiji (rolling ball radius = 10). The correlation coefficient was then computed in MATLAB.

Data analysis – blinded manual classification. All images to be classified were combined into a single data set. First, the user was given instructions on how to use the software and shown sample images that typified each category. Next, the user classified 20 images in a practice round, using a custom MATLAB GUI; these responses were not recorded. The user was then asked to sort each image in the data set into one of the categories, with the option to skip images they felt could not be classified. All images in the combined data set were shuffled and presented to the user in a random order, with no information about which experimental condition they came from.

Data analysis – correlation between filament speed and cytokinesis. FtsZ filament average velocities and constriction times were obtained from kymographs as described above (see "Correlation between FtsAZ motion and cytokinesis rates" and "Data analysis – kymographs"). Filament velocities versus constriction times were plotted using MATLAB. An exponential fit to the data was generated in MATLAB.

Data analysis – single cell growth rates. Wild type (PY79), FtsZ(D213A) (10 μM IPTG, strain bAB273) and FtsZ(T111A) (strain bAB270) cells were grown in LB at 37°C, placed onto LB+2% agarose pads and imaged with phase contrast for 90 minutes at 2 minute intervals. Individual cell growth was analyzed by a custom MATLAB program. First, the area of the cells was measured based on the segmentation of phase contrast images. Cells were then tracked over time. The growth rate of each cell is calculated by the slope of the linear fit of the natural logarithm of total areas. For each linear fit of the total area of cells, the R squared threshold is set to 0.95.

Sequences of Fluorescent Proteins, Tags and Linkers

msfGFP

ATGCGAAAAGGGGAAGAATTGTTTACAGGCGTAGTACCGATATTAGTTGAGCTGGA
TGGAGATGTTAACGGACACAAGTTTTCCGTACGCGGAGAGGGAGAAGGCGATGCCA
CCAATGGCAAACTCACCCTTAAATTTATTTGTACGACAGGCAAGCTACCAGTGCCGT
GGCCTACATTGGTCACTACACTCACGTATGGTGTGCAATGCTTTGCAAGATATCCCG
ACCACATGAAGCAACATGACTTTTTCAAATCAGCCATGCCTGAAGGATATGTCCAAG
AAAGGACTATTAGCTTTAAGGACGACGGCACCTACAAAACACGCGCTGAAGTCAAA
TTCGAAGGTGATACGTTAGTTAATCGTATCGAACTGAAAGGTATAGACTTTAAAGAA
GATGGAAATATCCTGGGGCATAAGTTGGAGTACAATTTCAACAGCCATAACGTATA
CATCACAGCTGACAAGCAGAAAAATGGCATTAAAGCAAATTTCAAAATCAGACATA
ACGTTGAAGATGGGTCAGTTCAGCTTGCGGATCATTATCAACAGAACACACCGATTG
GCGATGGTCCGGTGTTACTACCTGATAACCATTATCTGTCGACTCAGAGTAAACTGT
CTAAAGATCCAAATGAAAAACGGGACCACATGGTCCTTTTAGAGTTTGTGACGGCA
GCTGGGATTACGCATGGAATGGATGAACTTTACAAATAA

mNeonGreen
ATGGTTTCGAAAGGAGAGGAGGATAATATGGCTAGCCTCCCAGCGACCCACGAACT
GCATATTTTTGGCAGCATTAATGGCGTTGACTTTGATATGGTGGGGCAGGGAACAGG
GAACCCTAACGATGGCTATGAGGAGCTCAATCTCAAGAGTACAAAAGGAGATTTGC
AATTTTCACCTTGGATCCTGGTTCCGCATATTGGCTACGGCTTTCATCAATACTTGCC
TTATCCGGACGGCATGTCCCCGTTCCAAGCTGCGATGGTGGATGGTTCTGGGTACCA
GGTGCACCGTACTATGCAGTTTGAGGACGGTGCCTCACTGACGGTCAACTATAGATA
TACTTATGAAGGCTCACACATTAAGGGTGAGGCCCAAGTTAAAGGAACAGGGTTTC
CTGCGGATGGACCGGTAATGACAAACAGTTTAACCGCTGCGGACTGGTGTCGCTCG
AAAAAAACATACCCAAACGATAAAACGATCATCTCGACCTTCAAATGGAGCTATAC
TACGGGCAACGGCAAACGCTATCGTTCCACAGCACGCACGACTTATACGTTTGCTAA
ACCGATGGCCGCAAACTACCTCAAAAATCAACCTATGTACGTGTTCAGAAAAACCG
AGTTAAAACATTCAAAAACGGAACTTAATTTTAAAGAGTGGCAAAAGGCGTTTACA
GACGTGATGGGTATGGATGAACTCTATAAGTGA

HaloTag
ATGGCAGAAATCGGTACTGGCTTTCCATTCGACCCGCATTATGTGGAAGTCCTGGGC
GAGAGAATGCATTACGTTGACGTGGGTCCGAGAGATGGAACTCCGGTCCTTTTTCTG
CACGGGAATCCTACAAGCTCTTATGTTTGGCGCAATATCATCCCTCATGTAGCTCCG
ACGCATCGCTGTATTGCGCCGGACCTGATTGGTATGGGAAAATCTGATAAACCAGAC
CTGGGTTACTTTTTCGATGATCATGTGCGTTTCATGGATGCCTTCATTGAGGCATTAG
GGCTTGAAGAAGTCGTCTTGGTGATTCATGATTGGGGCTCAGCTCTGGGATTTCACT
GGGCTAAAAGAAATCCTGAACGCGTAAAAGGCATCGCGTTTATGGAGTTCATTCGTC
CAATTCCGACTTGGGATGAATGGCCTGAGTTCGCGAGAGAAACATTTCAAGCATTTC
GCACGACCGATGTAGGCCGGAAGTTAATCATCGATCAGAATGTCTTTATCGAAGGG
ACATTGCCGATGGGAGTCGTTCGTCCGTTAACAGAAGTCGAAATGGATCACTATAGA
GAACCTTTTCTTAATCCTGTGGACAGAGAGCCGCTGTGGCGGTTTCCGAACGAACTG
CCGATTGCAGGCGAGCCTGCTAACATTGTAGCGCTGGTTGAAGAGTATATGGATTGG
CTTCATCAGTCTCCAGTTCCGAAGTTATTGTTTTGGGGTACGCCTGGCGTGCTTATTC
CACCGGCCGAAGCGGCACGTTTGGCAAAAAGCCTGCCAAATTGCAAAGCCGTTGAC
ATTGGCCCTGGACTTAACTTGCTTCAAGAGGATAACCCGGACTTAATCGGGAGCGAA
ATTGCCCGGTGGCTTTCTACCTTAGAAATCAGCGGCTAG

15aa Linker A
CTCGAGGGATCTGGCCAGGGACCGGGCTCAGGCCAAGGAAGCGGC

15aa Linker B
CTTGAGGGTAGCGGACAAGGTCCTGGATCTGGTCAAGGCAGTGGG

Strain Construction

ME7 [*pbp2B::mNeonGreen-15aa-pbp2B*] was created by transforming PY79 with a Gibson assembly consisting of 4 fragments: 1) PCR with primers oME32 and oME22 and PY79 genomic DNA template (containing the region upstream of the *pbp2B* gene); 2) PCR with primers oZB46 and oZB47 and bMK93 genomic DNA template (containing the construct of first 30 bp

mNeonGreen-cat cassette-P_{xylA} *promoter-mazF gene-*P_{veg} *promoter*); 3) PCR with primers oZB33 and oZB34 and the synthetic *mNeonGreen* gene as template (ordered from IDT, see fluorophore sequences section); 4) PCR with primers oME20 and oME21 and PY79 genomic DNA template (containing the *pbp2B* gene). Transformations were plated on LB-Cm plates with 2% glucose and incubated at 37°C. Transformants were grown in LB with 2% glucose until OD_{600} ~ 0.5, plated on LB plates with 2% xylose, and incubated at 37°C. Colonies were then patched onto LB, LB-Cm and LB-Xylose plates and candidates that were sensitive to Cm but resistant to xylose were stocked and confirmed by PCR and sequencing.

bGS3 [*pbp2B::erm-*$P_{hyperspank}$*-mNeonGreen-15aa-pbp2B*] was created by transforming PY79 with a Gibson assembly consisting of 3 fragments: 1) PCR with primers oAB81 and oAB82 and PY79 genomic DNA template (containing the region upstream of the *pbp2B* gene); 2) PCR with primers oJM29 and oMD232 and bMD352 genomic DNA template (containing the construct *erm-*$P_{hyperskpank}$); 3) PCR with primers oAB137 and oAB87 and ME7 genomic DNA template (containing the *mNeonGreen-15aa-pbp2B* fusion). Transformations were plated on LB-MLS plates with 100 µM IPTG and colonies were patched onto LB and LB+IPTG plates. Candidates that presented resistance to MLS and IPTG dependence were confirmed by PCR and sequencing.

bGS28 [*pbp2B::erm-Phyperspank-HaloTag-15aa-pbp2B*] was created by transforming PY79 with a Gibson assembly consisting of 4 fragments: 1) PCR with primers oAB81 and oAB82 and PY79 genomic DNA template (containing the region upstream of the *pbp2B* gene); 2) PCR with primers oJM29 and oMD232 and bMD352 genomic DNA template (containing the construct *erm-*$P_{hyperskpank}$); 3) PCR with primers oGS7 and oAB14 and the synthetic *HaloTag* gene as template (ordered from DNA 2.0, see fluorophore sequences section); 4) PCR with primers oME20 and oAB87 and PY79 genomic DNA template (containing the *pbp2B* gene). Transformations were plated on LB-MLS plates with 100 µM IPTG and colonies were patched onto LB and LB+IPTG plates. Candidates that presented resistance to MLS and IPTG dependence were confirmed by PCR and sequencing.

bGS60 [*pbp2B::erm-Phyperspank-HaloTag-15aa-pbp2B, ftsZΩftsZ(T111A) (tet)*] was created by transforming bGS28 with genomic DNA from AB62 (a gift from Frederico Gueiros Filho).

bGS90 [*pbp2B::erm-Phyperspank-HaloTag-15aa-pbp2B, amyE::erm-*$P_{hyperspank}$*-ftsAZ(D213A)*] was created by transforming bGS28 with genomic DNA from bAB215.

bGS31 [*pbp2B::erm-Phyperspank-HaloTag-15aa-pbp2B, ftsZ::mNeonGreen-15aa-ftsZ]* was created by transforming bAB185 with genomic DNA from bGS28.

bAB94 [*amyE::erm-*$P_{hyperspank}$*-ftsA*] was created by transforming PY79 with a Gibson assembly consisting of 3 fragments: 1) PCR with primers oMD191 and oMD232 and bMD352 genomic DNA template (containing the region upstream of the *amyE* gene, the *erm* cassette and the $P_{hyperspank}$ promoter); 2) PCR with primers oAB78 and oAB93 and PY79 genomic DNA template (containing the *ftsA* gene); 3) PCR with primers oMD196 and oMD197 and PY79 genomic DNA template (containing the region downstream of *amyE*).

bAB96 [*amyE::erm-*$P_{hyperspank}$*-ftsZ*] was created by transforming PY79 with a Gibson assembly consisting of 3 fragments: 1) PCR with primers oMD191 and oMD232 and bMD352 genomic DNA template (containing the region upstream of the *amyE* gene, the *erm* cassette and the $P_{hyperspank}$ promoter); 2) PCR with primers oAB95 and oAB94 and PY79 genomic DNA template (containing the *ftsA* gene); 3) PCR with primers oMD196 and oMD197 and PY79 genomic DNA template (containing the region downstream of *amyE*).

bAB98 [*amyE::erm-*$P_{hyperspank}$*-ftsAZ*] was created by transforming PY79 with a Gibson assembly consisting of 3 fragments: 1) PCR with primers oMD191 and oMD232 and bMD352 genomic DNA template (containing the region upstream of the *amyE* gene, the *erm* cassette and the $P_{hyperspank}$ promoter); 2) PCR with primers oAB78 and oAB94 and PY79 genomic DNA template (containing the *ftsAZ* operon); 3) PCR with primers oMD196 and oMD197 and PY79 genomic DNA template (containing the region downstream of *amyE*).

bAB146 [*amyE::erm-*$P_{hyperspank}$*-mNeonGreen-15aa-pbp2B*] was created by transforming PY79 with a Gibson assembly consisting of 3 fragments: 1) PCR with primers oMD191 and oMD232 and bMD352 genomic DNA template (containing the upstream region to *amyE* gene, the *erm* cassette and the $P_{hyperspank}$ promoter); 2) PCR with primers oAB137 and oAB134 and ME7 genomic DNA template (containing the mNeonGreen-15aa-pbp2B construct); 3) PCR with primers oMD196 and oMD197 and PY79 genomic DNA template (containing the region downstream to *amyE*).

bAB167 [*ftsA::ftsA-mNeonGreen(SW)*] was created by inserting mNeonGreen between helices 6 and 7 of FtsA, the equivalent of a sandwich fusion (SW) that proved to be functional for MreB-mCherry (*38*). PY79 cells were transformed with a Gibson assembly consisting of 7 fragments: 1) PCR with primers oAB74 and oAB75 and template PY79 genomic DNA (containing the region upstream of the *ftsAZ* promoters); 2) PCR with primers oJM28 and oJM29 and template pWX467a (containing the *erm* cassette); 3) PCR with primers oAB76 and oAB33 and template PY79 genomic DNA (containing the first 801 bp of the *ftsA* gene); 4) PCR with primers oAB135 and oAB136 and the synthetic *mNeonGreen* gene as template (ordered from IDT, see fluorophore sequences section); 5) PCR with primers oAB48 and oAB28 and template PY79 genomic DNA (containing the last 522 bp of the *ftsA* gene and the *ftsZ* region); 6) PCR with primers oJM28 and oJM29 and template pWX465a (containing the *cat* cassette); 7) PCR with primers oAB29 and oAB30 and template PY79 genomic DNA (containing the region downstream of *ftsAZ* terminators). After proper integration was confirmed by PCR and sequencing, the resistance cassettes were looped-out using pDR244 (containing Cre recombinase, a gift from David Rudner), and incubating transformed cells overnight at 30°C. Colonies were streaked onto LB, LB-MLS, LB-Cm and LB-Spec plates and incubated overnight at 45°C. After confirming that only LB plates presented colonies, the loop-outs were confirmed by PCR and sequencing.

bAB185 [*ftsZ::mNeonGreen-15aa-ftsZ*] was created by transforming PY79 with a Gibson assembly consisting of 7 fragments: 1) PCR with primers oAB74 and oAB75 and template PY79 genomic DNA (containing the region upstream of the *ftsAZ* promoters); 2) PCR with primers oJM28 and oJM29 and template pWX467a (containing the *erm* cassette); 3) PCR with primers oAB76 and oAB139 and template PY79 genomic DNA (containing the region upstream of the *ftsZ* gene); 4) PCR with primers oZB33 and oZB34 and the synthetic *mNeonGreen* gene as template

(ordered from IDT, see fluorophore sequences section); 5) PCR with primers oAB140 and oAB28 and template PY79 genomic DNA (containing the *ftsZ* gene region); 6) PCR with primers oJM28 and oJM29 and template pWX465a (containing the *cat* cassette); 7) PCR with primers oAB29 and oAB30 and template PY79 genomic DNA (containing the region downstream of the *ftsAZ* terminators). After proper integration was confirmed by PCR and sequencing, the resistance cassettes were looped out by transforming the plasmid pDR244 (containing Cre recombinase and a temperature sensitive origin of replication, a gift from David Rudner), and incubating transformed cells overnight at 30°C. Colonies were streaked onto LB, LB-MLS, LB-Cm and LB-Spec plates and incubated overnight at 45°C to remove the plasmid. After confirming that only LB plates presented colonies, the loop-outs were confirmed by PCR and sequencing.

bAB199 [*ftsZ::mNeonGreen-15aa-ftsZ, amyE::erm-*$P_{hyperspank}$*-ftsA*] was created by transforming bAB185 with genomic DNA from bAB94.

bAB209 [*ftsZ::mNeonGreen-15aa-ftsZ, amyE::*P_{XylA}*-mciZ (cat)*] was created by transforming bAB185 with genomic DNA from AH93.

bAB213 [*ftsAZ::erm-ftsA-HaloTag(SW)-ftsZ-cat*] was created by inserting HaloTag between helices 6 and 7 of FtsA, the equivalent of a sandwich fusion (SW) that proved to be functional for MreB-mCherry (*38*). PY79 cells were transformed with a Gibson assembly consisting of 3 fragments: 1) PCR with primers oAB74 and oAB33 and template bAB163 genomic DNA (containing the region beginning upstream of the *ftsAZ* promoters and including the first 801 bp of the *ftsA* gene, *erm* cassette included); 2) PCR with primers oAB21 and oAB44 and the synthetic *HaloTag* gene as template (ordered from DNA 2.0, see fluorophore sequences section); 3) PCR with primers oAB48 and oAB30 and template bAB167 genomic DNA (containing the region from the last 522 bp of the *ftsA* gene to downstream of the *ftsAZ* terminators, *cat* cassette included). Proper integration was confirmed by PCR and sequencing.

bAB215 [*amyE::erm-*$P_{hyperspank}$*-ftsAZ(D213A)*] was created by transforming PY79 with a Gibson assembly consisting of 3 fragments: 1) PCR with primers oMD191 and oMD232 and bMD352 genomic DNA template (containing the region upstream of the *amyE* gene, the *erm* cassette and the $P_{hyperspank}$ promoter); 2) PCR with primers oAB78 and oAB124 and bAB98 genomic DNA template (containing the first 2047 bp of the *ftsAZ* operon, inserting the mutation GCT at bp 638 of the *ftsZ* gene); 3) PCR with primers oMD123 and oMD197 and bAB98 genomic DNA template (containing the last 529 bp of the *ftsZ* gene, inserting the mutation GCT at the 638 bp position of the *ftsZ* gene, and the region downstream of *amyE*).

bAB217 [*amyE::erm-*$P_{hyperspank}$*-ftsA-mNeonGreen(SW)-ftsZ(D213A)*] was created by transforming PY79 with a Gibson assembly consisting of 3 fragments: 1) PCR with primers oMD191 and oMD232 and bMD352 genomic DNA template (containing the region upstream of the *amyE* gene, the *erm* cassette and the $P_{hyperspank}$ promoter); 2) PCR with primers oAB78 and oAB124 and bAB163 genomic DNA template (containing the first 2845 bp of the *ftsA-mNeonGreen(SW)-ftsZ* operon, inserting the mutation GCT at bp 638 of the *ftsZ* gene); 3) PCR with primers oAB123 and oMD197 and bAB98 genomic DNA template (containing the last 529 bp of the *ftsZ* gene, inserting the mutation GCT at the 638 bp position of the *ftsZ* gene, and the region downstream of *amyE*).

bAB219 [*amyE::erm-*$P_{hyperspank}$*-ftsA-mNeonGreen-15aa-ftsZ*] was created by transforming PY79 with a Gibson assembly consisting of 3 fragments: 1) PCR with primers oMD191 and oMD232 and bMD352 genomic DNA template (containing the region upstream of the *amyE* gene, the *erm* cassette and the $P_{hyperspank}$ promoter); 2) PCR with primers oAB78 and oAB94 and bAB185 genomic DNA template (containing the *ftsA-mNeonGreen-15aa-ftsZ* operon); 3) PCR with primers oMD196 and oMD197 and PY79 genomic DNA template (containing the region downstream of *amyE*).

bAB221 [*ftsZ::mNeonGreen-15aa-ftsZ, amyE::erm-*$P_{hyperspank}$*-ftsA-mNeonGreen-15aa-ftsZ*] was created by transforming bAB185 with genomic DNA from bAB219.

bAB229 [*ftsAZ::erm-ftsA-HaloTag(SW)-mNeonGreen-15aa-ftsZ-cat*] was created by transforming PY79 with a Gibson assembly consisting of 2 fragments: 1) PCR with primers oAB74 and oAB44 and template bAB213 genomic DNA (containing the region from upstream of the *ftsAZ* promoters to the end of the *HaloTag* gene, *erm* cassette included); 2) PCR with primers oAB48 and oAB30 and template bAB181 genomic DNA (containing the region from the last 522 bp of the *ftsA* gene to downstream of the *ftsAZ* terminators, *cat* cassette included). Proper integration was confirmed by PCR and sequencing.

bAB248 [*ftsZ::mNeonGreen-15aa-ftsZ, amyE::*$P_{hyperspank}$*-minCD (spc)*] was created by transforming bAB185 with genomic DNA from JB60 (a gift from Frederico Gueiros Filho).

bAB270 [*pbp2B::mNeonGreen-15aa-pbp2B, ftsZΩftsZ(T111A) (tet)*] was created by transforming ME7 with genomic DNA from AB62 (a gift from Frederico Gueiros Filho).

bAB271 [*pbp2B::mNeonGreen-15aa-pbp2B, ftsZΩftsZ(G106S) (tet)*] was created by transforming ME7 with genomic DNA from Z-84 (a gift from Frederico Gueiros Filho).

bAB272 [*pbp2B::mNeonGreen-15aa-pbp2B, amyE::erm-*$P_{hyperspank}$*-ftsAZ*] was created by transforming ME7 with genomic DNA from bAB98.

bAB273 [*pbp2B::mNeonGreen-15aa-pbp2B, amyE::erm-*$P_{hyperspank}$*-ftsAZ(D213A)*] was created by transforming ME7 with genomic DNA from bAB215.

bAB274 [*pbp2B::mNeonGreen-15aa-pbp2B, amyE::*P_{XylA}*-mciZ (cat)*] was created by transforming ME7 with genomic DNA from AH93.

bAB281 [*amyE::erm-*$P_{hyperspank}$*-ftsA-mNeonGreen-15aa-ftsZ, ftsZΩftsZ(T111A) (tet)*] was created by transforming bAB219 with genomic DNA from AB62 (a gift from Frederico Gueiros Filho).

bAB282 [*amyE::erm-*$P_{hyperspank}$*-ftsA-mNeonGreen-15aa-ftsZ, ftsZΩftsZ(G106S) (tet)*] was created by transforming bAB219 with genomic DNA from Z-G106S (a gift from Frederico Gueiros Filho).

bAB285 [*pbp2B::mNeonGreen-15aa-pbp2B, amyE::*$P_{hyperspank}$*-minCD (spc)*] was created by transforming ME7 with genomic DNA from JB60 (a gift from Frederico Gueiros Filho).

bAB310 [*pbp2B::mNeonGreen-15aa-pbp2B, amyE::erm-*$P_{hyperspank}$*-ftsA*] was created by transforming ME7 with genomic DNA from bAB94.

SH013 [*trpC2, ftsZ:: ftsZ-GFP::cat*] was created by transforming *B. subtilis* 168CA [*trpC2*] with genomic DNA from PL642 (a gift from Petra Anne Levin).

SH033 [*trpC2, ftsZ:: ftsZ-GFP::cat, Δhag::aph(Kan)*] was created by transforming SH013 with genomic DNA from PB5250 (obtained from BGSC catalogue number 1A842).

SH41 [*ftsZ::mNeonGreen-15aa-ftsZ, Δhag::aph (Kan*)] was created by transforming bAB185 with genomic DNA from PB5250 (obtained from BGSC catalogue number 1A842).

Supplemental Figures

Figure S1: The FDAA labeling pattern is independent of the FDAA type or the sequence in which they are used

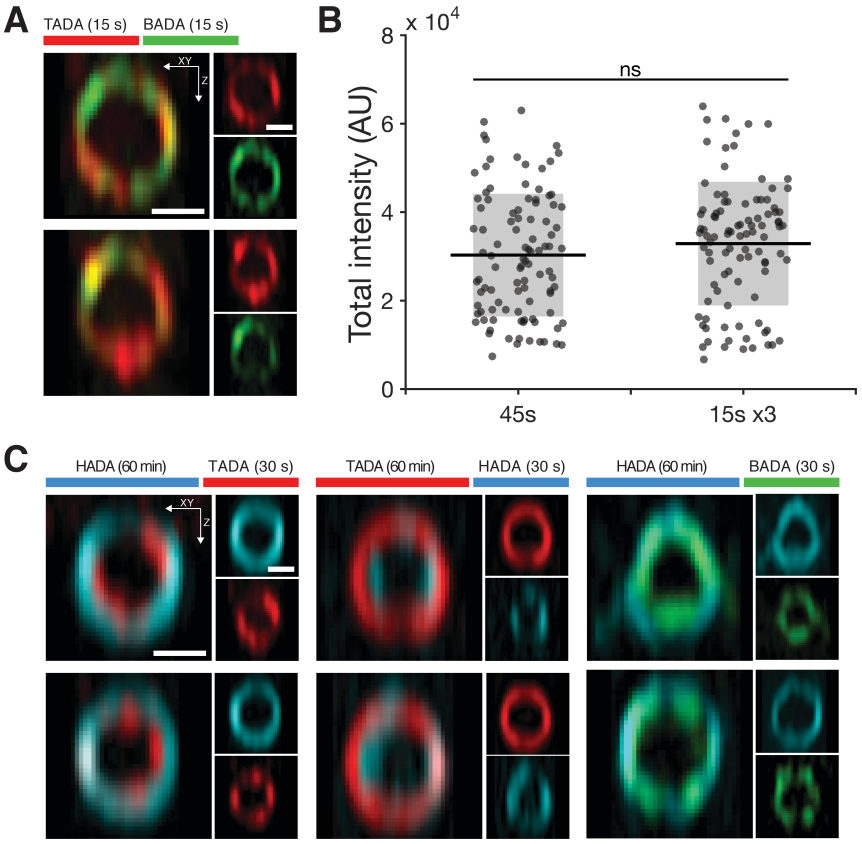

A Sequential short-pulse labeling of FDAAs with reversed color sequence compared to Fig. 1B. This demonstrates the pattern of FDAA sequential labeling is independent of the sequence of FDAA labeling.

B Labeling cells with FDAAs for one 45-second pulse yields the same label intensity as labeling for three sequential 15-second pulses. This indicates that FDAA pulses of different durations are comparable, and that repeated pulse labeling with FDAAs is non-perturbing. ns: the comparison is not statistically significant by t-test.

C FDAA sequential labeling using different orders of dyes (indicated in diagrams). Discrete spots of FDAA labeling were seen in short-pulse labeling regardless of what FDAA color was used for the pulse. Images were background subtracted in Fiji (rolling ball radius = 10).

Colored bars indicate the time course of FDAA labeling in each experiment. All images were taken with 3D-SIM. Scale bars = 0.5 μm.

Figure S2: Quantitation of FDAA labeling from 3D-SIM data

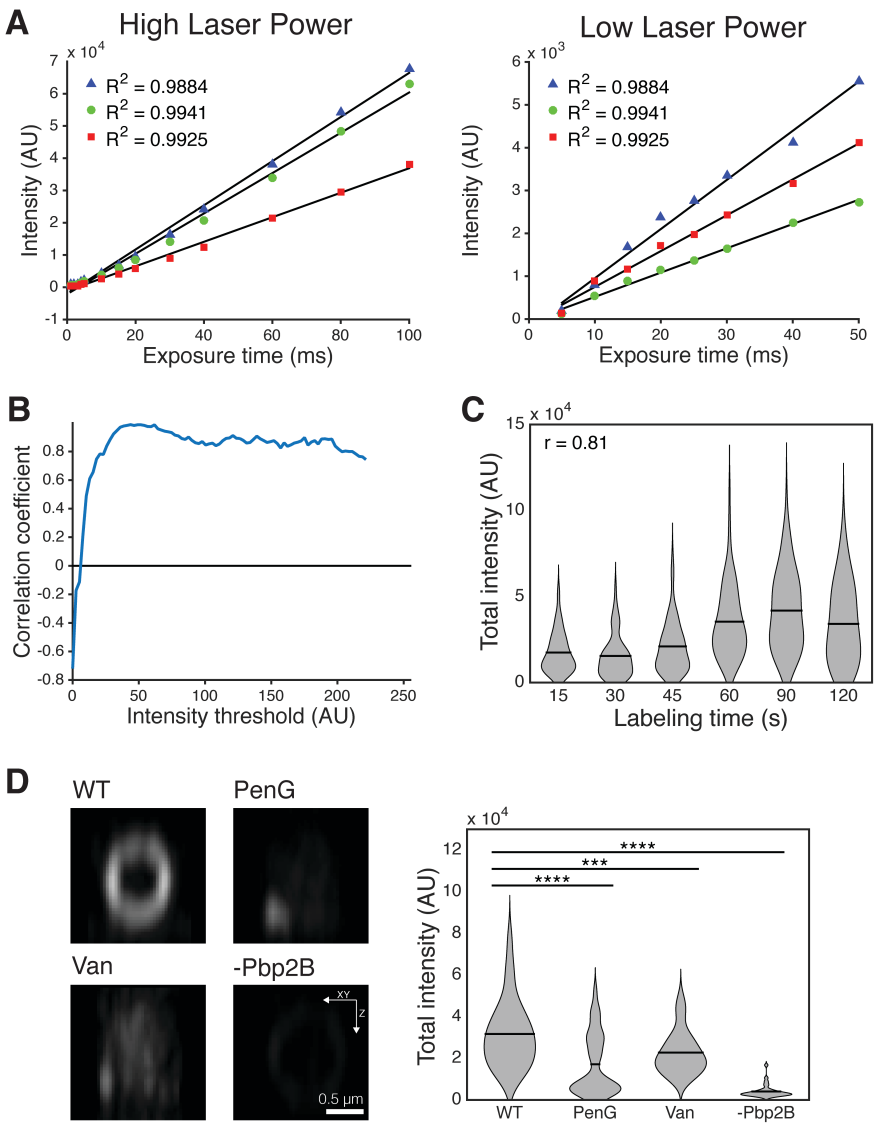

A The fluorescence intensity measured from 3D-SIM imaging varies linearly with exposure times both at high (left) and low (right) laser powers, validating intensity-based quantitation. Plot shows the maximum intensity of TetraSpeck beads measured at varying exposure times for three different fields of view. Black lines are linear fits to each field of view.

B The area of FDAA-labeled features at the septum increases with increased labeling time (as in Fig. 1D) independent of the threshold cutoff used to binarize images. Labeled area is measured as the number of pixels in each region above a chosen intensity threshold. Fig. 1D shows that for one such threshold (45 units) FDAA labeling time and average labeled area are positively correlated. This graph shows the correlation coefficients for the complete range of possible threshold choices, indicating that this correlation holds regardless of threshold choice, except at the extreme values.

C The total amount of FDAA labeling at the septum increases with labeling time. Total amount of labeling is calculated as the sum of the fluorescence intensity in each image; distribution shown as violin plots, black lines: means of the distributions. r: correlation coefficient of means.

D Disruption of cell wall synthesis causes decreased FDAA labeling at the septum. To decrease cell wall synthesis, cells were treated with 4 μg/ml Vancomycin for 3 min (Van), 50 μg/ml Penicillin G for 3 min (PenG), or Pbp2B was depleted for 3 hours. Following perturbations, cells

were labeled with 2 mM TADA for 2 minutes. (Left) representative TADA images for each condition. Representative images shown are those with the median intensity of their distribution. (Right) total FDAA intensity for each condition. Black lines indicate the mean.

Figure S3: Viability and fitness of native fusions

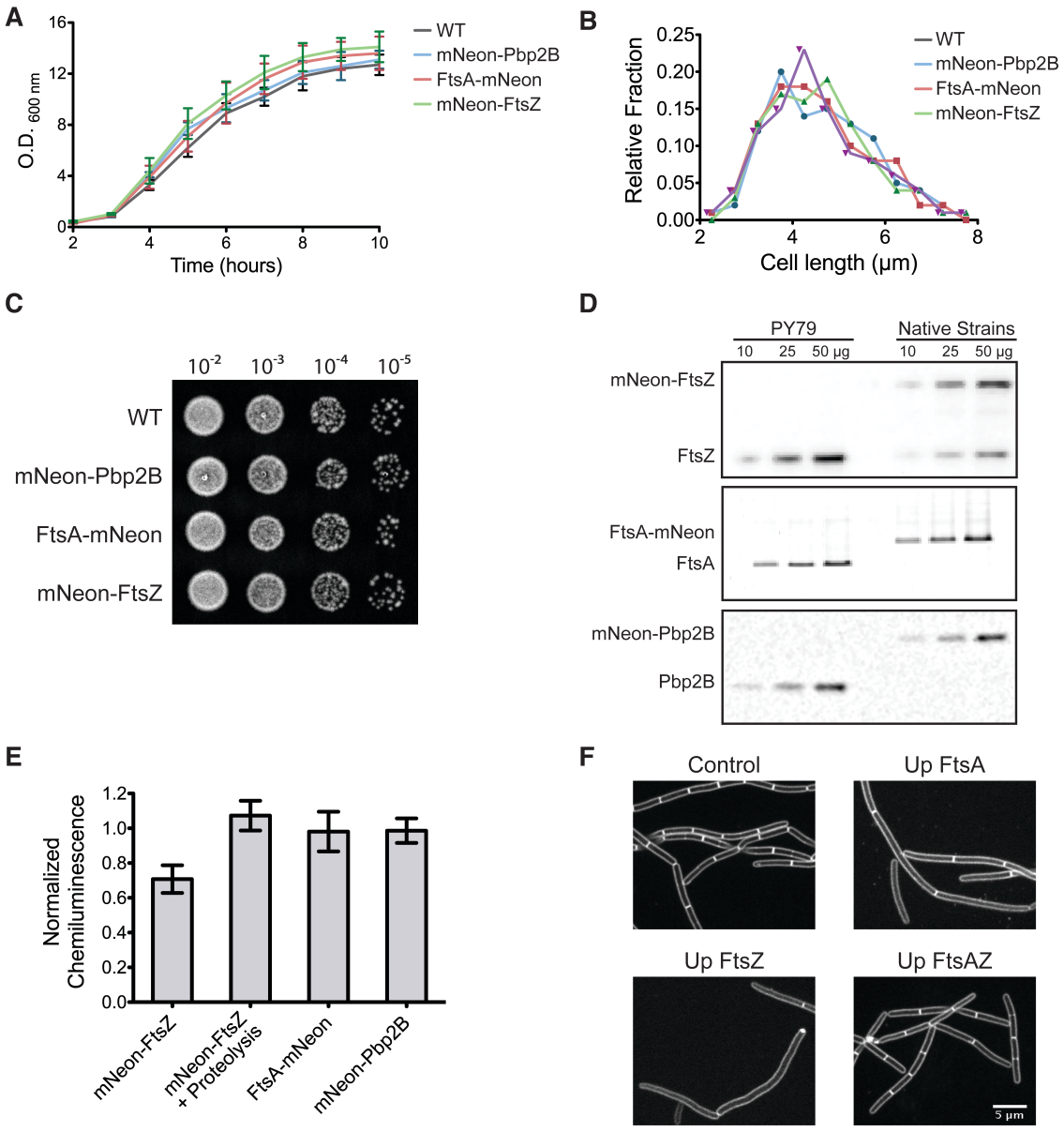

Native mNeonGreen fusions of Pbp2B (strain ME7), FtsA (strain bAB167), and FtsZ (strain bAB185) have similar fitness and protein levels compared to wild type cells (strain PY79).

A Growth curves of native fusion strains. Cells were grown in triplicate in LB until O.D.$_{600}$ < 1.0, and then diluted to O.D. $_{600}$ = 0.1. Aliquots were taken every hour and O.D.$_{600}$ was measured in a plate reader (Synergy HT plate reader, Bio-Tek).

B Cell length distributions. Cells were grown until mid-exponential phase in LB, concentrated and incubated for 1 minute with 1 μg/ml of FM5-95 dye, and imaged in a confocal spinning disk microscope. Cell length was measured using 250 cells for each strain.

C Cell viability from spot dilutions. Cells were grown until $O.D._{600}$ ~ 1.0 in LB, 5 µl of each culture was spotted from serial dilutions on LB plates, and incubated for 12 hours.

D Relative protein levels of native fusions compared to wild type assayed by Western blotting. Different lysate dilutions of each strain carrying its respective native fusion were blotted side by side with PY79 control. Cells were incubated with specific polyclonal antibodies for FtsZ, FtsA and Pbp2B, respectively. Bands were probed and visualized using a chemiluminescence system.

E Relative quantification of native mNeonGreen fusions. Mean values were obtained from the average of 3 independent experiments, and normalized to the measurements of the respective untagged band from PY79. FtsA-mNeonGreen:FtsA and mNeonGreen-Pbp2B:Pbp2B ratios show similar protein levels (0.98±0.11 and 0.99±0.07, respectively). For the mNeonGreen-FtsZ fusion, considerably lower mNeonGreen-FtsZ:FtsZ ratios were observed (0.71±0.08). However, a proteolysis product from mNeonGreen-FtsZ construct was observed in all blots, and the sum of the intensities of mNeonGreen-FtsZ and its proteolysis product gave a balanced ratio (1.07±0.09).

F Increased FtsAZ levels have no measurable effect on fitness or cell division, indicating that while overexpression of either FtsA or FtsZ alone may be toxic, balanced expression of both causes no observable cellular defects. Membrane staining of cells overexpressing a second copy of *ftsZ* (strain bAB96, bottom left panel), *ftsA* (bAB94, top right panel) or *ftsAZ* (bAB98, bottom right panel). The control (top left panel) is a representative image of bAB96 cells without FtsZ overexpression. Cells were grown in LB until mid-exponential phase, diluted into fresh medium with 100 µM IPTG (or 0 µM IPTG as a control for each culture) and grown for more 2 hours prior imaging. Images were acquired on a spinning-disk confocal microscope after cells were incubated with 1 µg/ml of FM5-95 dye for 30 seconds at room temperature. Because the overexpression of either FtsZ or FtsA alone affected cell length and width, most of our experiments using inducible constructs were performed by expressing both FtsA and FtsZ together, which had no such effects. Growth rates of cells overexpressing FtsAZ are shown in S7A (brown curve), with no observable change from wildtype.

Figure S4: Imaging FtsZ in microholes

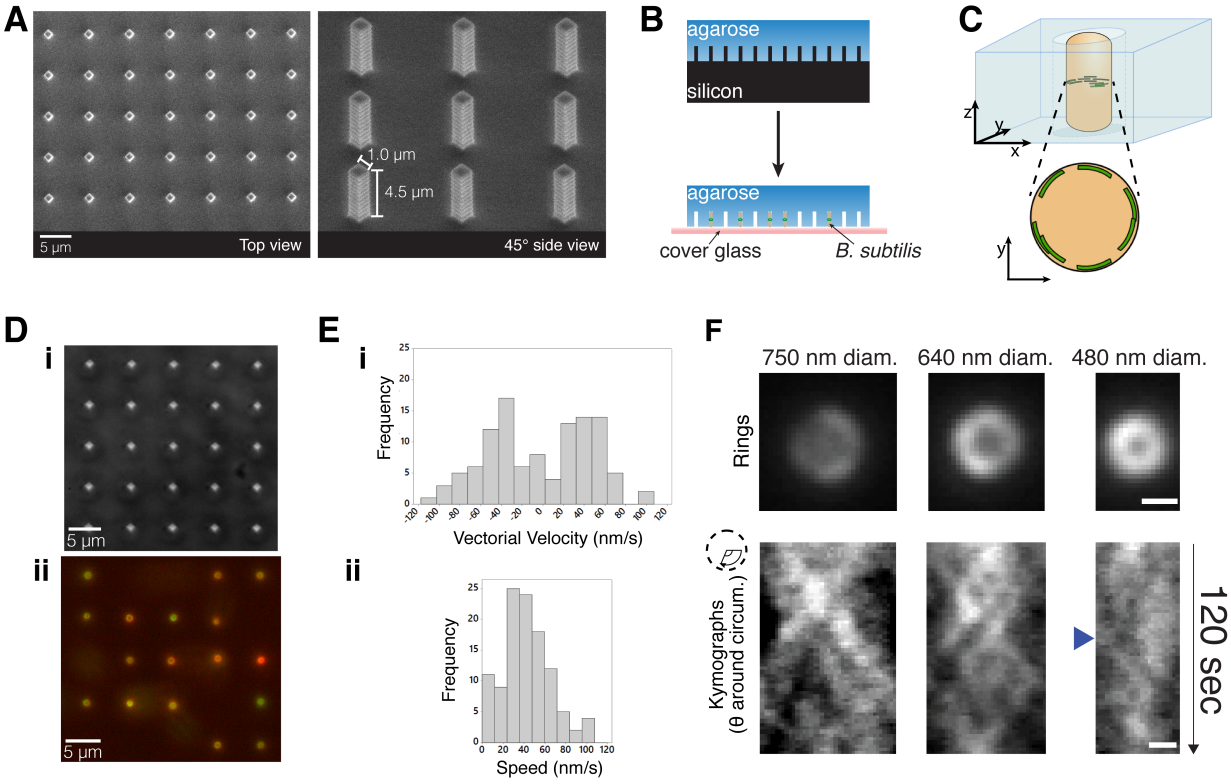

A Scanning electron microscopy images of silicon micropillars nanofabricated through electron-beam lithography and reactive-ion etching.

B Schematic of the stamping process to produce agarose pads containing microholes.

C Schematic of *B. subtilis* in microholes. FtsZ filaments are shown in green.

D (i) Brightfield images of microholes without bacteria. (ii) Widefield epifluorescence images of *B. subtilis* (SH33) inoculated in microholes. Green indicates GFP-FtsZ, red indicates FM4-64-labeled cell membrane.

E Quantification of mNeonGreen-FtsZ filament dynamics in actively constricting vertically immobilized cells**.** FtsZ filaments move in both directions with equal probability. Vectorial velocities (i) and speeds (ii) of mNeonGreen-FtsZ filaments (strain SH41). Mean filament speed was 42 nm ± 23 nm/sec (mean ± S.D., N = 110). 25% of filaments were immobile (speed of ~ 0 nm/s).

F A FtsZ-GFP fusion has similar dynamics compared to mNeonGreen-FtsZ. Vertically immobilized cells (strain SH33) display multiple FtsZ-GFP filaments with independent directional motion around the division site. (top) Cropped rings in early (left), mid (center), and late (right) divisional stages. (bottom). Blue arrow indicates start of a directional FtsZ track. Scale bars = 0.5 µm**.**

Figure S5: Divisome imaging and particle tracking

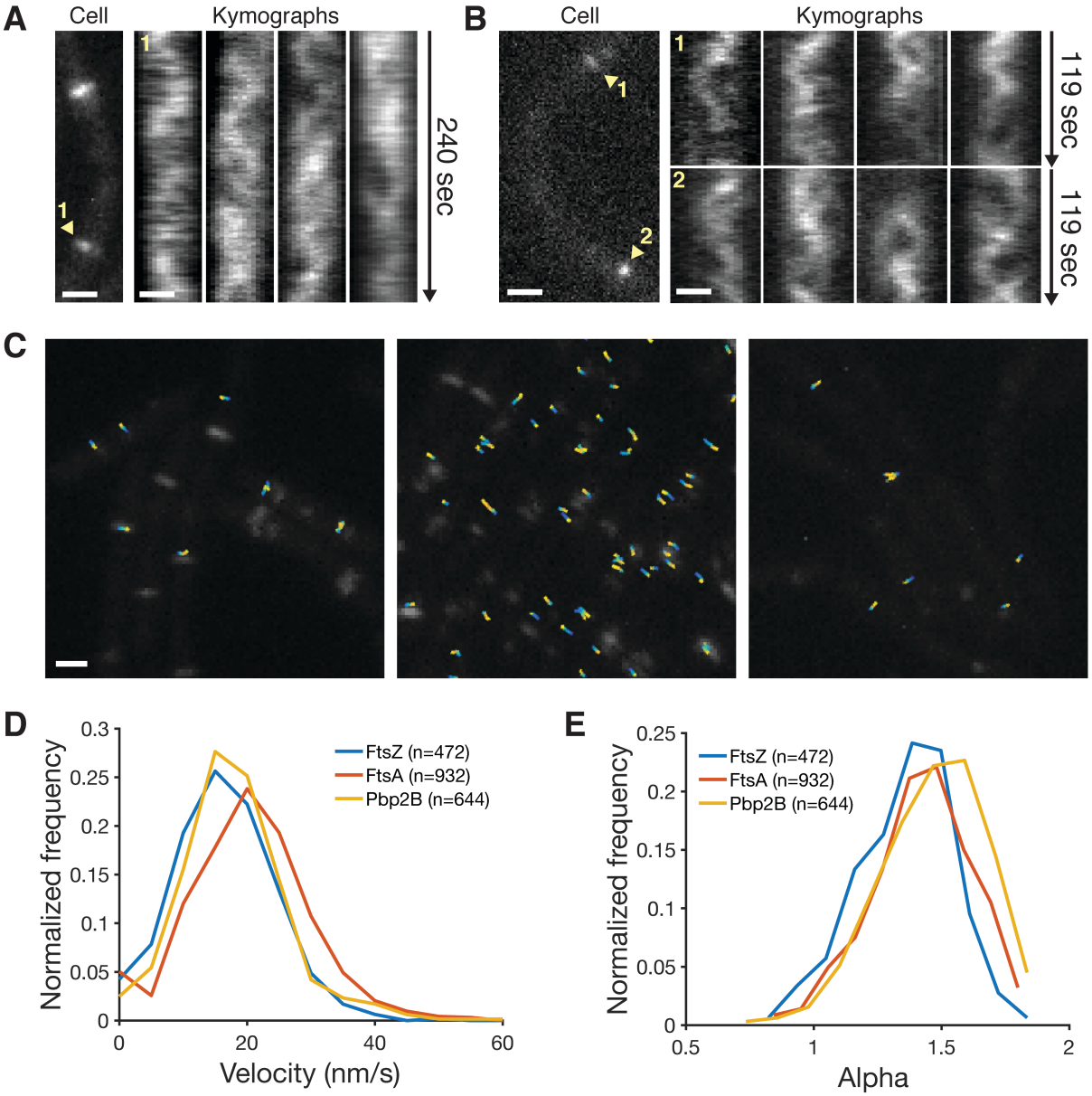

Figure S5 (cont.): Divisome imaging and particle tracking

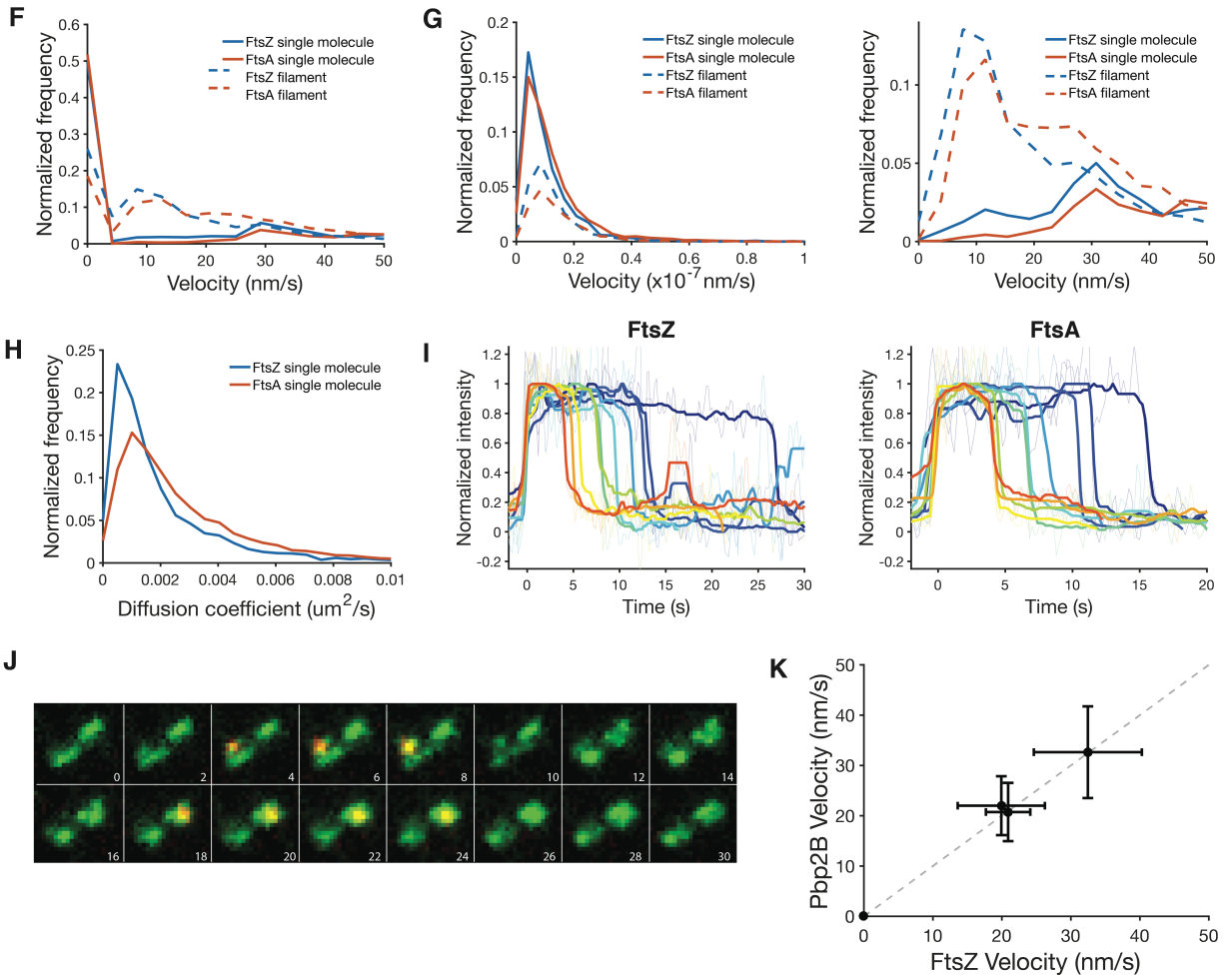

A Pbp2B-mNeonGreen expressed at native levels (ME7) shows Pbp2B motion at the Z ring, imaged by TIRF microscopy. Pbp2B can be seen throughout the cell, but localizes preferentially to the Z ring. Indicated kymograph (right) was drawn at the arrowhead. Scale bars: 1 µm (cell), 0.5 µm (kymograph).

B Pbp2B-mNeonGreen expressed at low levels (bGS3) shows Pbp2B motion at the Z ring as imaged by TIRF microscopy. Cells were grown in 2 µM IPTG to induce low levels of Pbp2B expression. This decreased the overall signal density, allowing dynamics to be resolved more clearly. Kymographs are drawn at arrowheads. Scale bars: 1 µm (cell), 0.5 µm (kymograph).

C Particle tracking shows directional motion of FtsZ filaments (left), FtsA filaments (center), and Pbp2B single molecules (right). mNeonGreen-FtsZ (bAB185), FtsA-mNeonGreen (bAB167), and Halo-Pbp2B (bGS31) labeled with 40 µM JF-549 were imaged by TIRF microscopy. Particles were identified and tracked using TrackMate and analyzed using custom MATLAB code. Tracks are overlaid on a frame from each time lapse, and are colored blue to yellow along their duration. Scale bar: 1 µm.

D Particle tracking shows that FtsA, FtsZ, and Pbp2B all move at the same speed. Particle tracks were filtered to select for directional motion, and velocity was calculated from fits of particle tracks to $MSD(t)=4D(t)+(Vt)^2$ (*15*). The small difference in the means of these distributions compared to the velocity distributions in Fig. 2G (velocity measurement by kymograph) is likely due to differences in the two methods of measuring velocity. However, the velocities of FtsA, FtsZ and Pbp2B agree with each other when assayed using two independent velocity measurements, reinforcing the conclusion that they move at the same speed.

E Distributions of the scaling coefficient α for particle tracks of FtsA, FtsZ, and Pbp2B indicates that they move directionally. α was calculated as described previously (*15*). This distribution of α values is consistent with directed motion ($1 < \alpha < 2$).

F Distributions of the velocity of unfiltered FtsZ and A particle tracks calculated from fits of (MSD vs t) to $MSD(t)=4D(t)+(Vt)^2$ for both single molecules (solid lines) and filaments (dashed lines). FtsA and FtsZ filament trajectories show a mobile population (visible as a second peak in the 10-20 nm/s region), whereas the motions of single molecules show a negligible value for directional motion ($\sim 10^{-8}$ nm/s).

G Detailed velocity distributions of FtsZ and FtsA single molecules and filaments. Left: Distributions of all velocities less than 10^{-7} nm/s, representing the non-moving population of particles. Right: Distributions of all velocities greater than 10^{-7} nm/s, representing the mobile population. Single molecules of FtsA and FtsZ have more non-moving particles and very few moving particles compared to filaments, indicating that, while filaments of FtsZ and FtsA move, single molecules do not.

H Distributions of the diffusion coefficients for unfiltered FtsZ and FtsA particle tracks calculated from fits of (MSD vs t) to $MSD(t)=4D(t)+(Vt)^2$. Single molecules of mNeonGreen-FtsZ (bAB219) and Halo-FtsA (bAB213) labeled with 100 pM JF-549 were imaged by TIRF microscopy. Particles were tracked and diffusion coefficients calculated as described above. The very low value of the diffusion coefficient is consistent with immobile particles, and similar to that of immobile class A PBPs measured in *E. coli* and *B. subtilis* (*39, 40*).

For panels F-H, n = 2,695 (FtsZ single molecules), 10,358 (FtsA single molecules), 4,718 (FtsZ filaments), 7,164 (FtsA filaments).

I Single-step photobleaching of FtsZ and FtsA single molecules. Intensity traces are aligned such that the frame in which the molecule appears is time = 0. Faded, thin lines show the raw data; the bold lines are data which has been filtered to reduce noise. The fluorescence signal drops to baseline in a single time step, indicating that these are single molecules.

J Simultaneous imaging of directionally-moving FtsZ filaments and immobile FtsA single molecules. Dual-color TIRF imaging of native levels of mNeonGreen-FtsZ (green) and single molecules of FtsA-HaloTag-JF549 (red). Images were taken at 2 second intervals with 250 ms exposure times.

K Pbp2B velocity correlates with FtsAZ filament velocity. JF549-HaloTag-Pbp2B single molecules were imaged under 5 different conditions, their velocities measured by kymographs and plotted against the FtsAZ filament velocity in that same condition. Pbp2B velocities (mean ± S.D.): wild type (strain bGS31, n = 152): 32.6 ± 9.1 nm/sec; FtsA overexpression (strain bAB310 with 20 μM IPTG, n = 87): 22.0 ± 5.8 nm/sec; FtsZ(D213A) (strain bGS90 with 100 μM IPTG): no motion detected; FtsZ(T111A) (strain bGS60, n = 108): 20.7 ± 5.8 nm/s; PC190723 treatment (strain bGS31 with 10 μM PC190723): no motion detected.

Figure S6: FDAA labeling with FtsAZ velocity perturbations

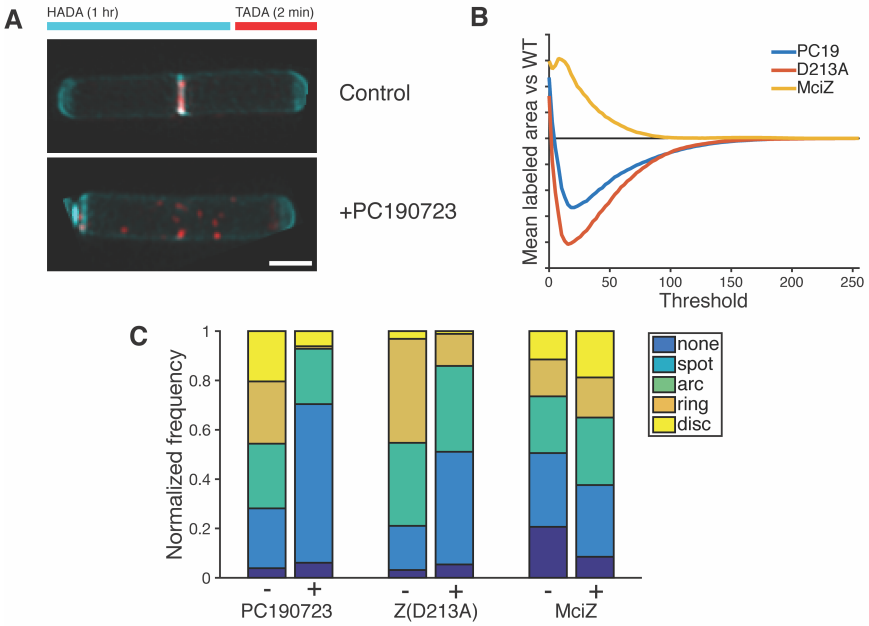

A Treatment with high concentrations of PC190723 causes PG synthesis to localize to small patches along the cell, mirroring the localization of FtsZ following similar treatment. Cells were treated with 10 µg/ml PC190723 for 10 minutes, and labeled with TADA as shown. A cell not treated with PC190723 that was labeled equivalently with FDAAs is shown for comparison. Scale bar: 1 µm.

B The trends observed in Fig. 4B are independent of threshold used for analysis. For each perturbation (PC190723, FtsZ(D213A), MciZ), data plotted is the mean FDAA-labeled area with perturbation minus the mean FDAA-labeled area without perturbation. Negative values of the curves indicate that the perturbation decreases labeled area, while positive values indicate that the perturbation increases labeled area. These measurements are consistent across all possible thresholds for labeling except extreme values, indicating that the trends reported in Fig. 4B are independent of threshold choice.

C Blinded classification of FDAA labeling under various FtsZ perturbations. This demonstrates that perturbations that decrease FtsZ velocity also cause more heterogeneous labeling (more spots and arcs, fewer complete rings), whereas perturbations that increase FtsZ velocity yield a more uniform distribution of FDAA signal. + indicates sample with perturbation, – indicates unperturbed sample for comparison. Note that the labeling and imaging conditions varied for the three experiments shown here, explaining the variation between the three unperturbed samples. See Table S1 for details.

Figure S7: Perturbation of FtsAZ dynamics affects cytokinesis time, but not growth rate

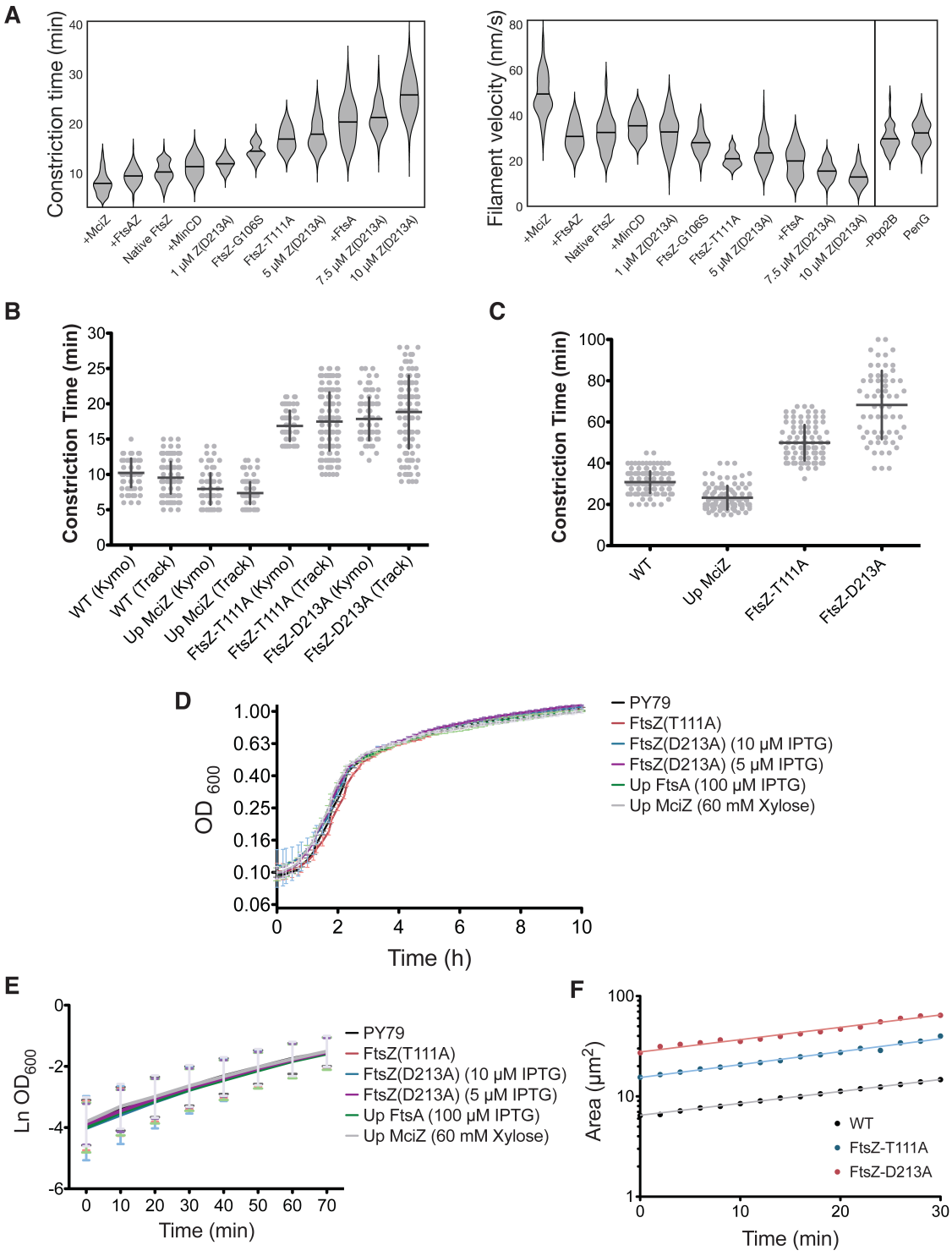

A Violin distributions of (left) mNeonGreen-Pbp2B constriction times (measured from kymographs) and (right) FtsAZ filament velocities under different conditions. Cells were grown and imaged as described in methods.

B Comparison between constriction times of Pbp2B rings measured by kymograph (Kymo) and automated tracking (Track) analysis. Scatter plot of constriction time distributions was obtained as described in methods; statistics are shown in Table S4.

C Distribution of constriction times obtained from cells under slow growth conditions ($S7_{50}$-glucose at 25°C). Perturbations that changed FtsAZ filament motion and constriction times in rich media at 37°C had the same effect in minimal media at 25˚C, either slowing down (FtsZ(T111A) - strain bAB270, FtsZ(D213A) - strain bAB273 with 10 µM IPTG) or accelerating (MciZ overexpression - strain bAB274 with 5 µL of 3 M xylose on top of the pad) the rate of cytokinesis.

D Bulk growth curves of cells under all FtsZ perturbations that significantly changed constriction rates. Cells were grown in LB until $OD_{600} < 1.0$, and then diluted to $OD_{600} = 0.1$ and split into 8 replicates. Growth curves were taken in a plate reader (Epoch-2 plate reader, Biotek) with continuous shaking at 37°C.

E Linear segments from growth curves in D (40 to 110 minutes). Curves were converted into a $\ln(OD_{600})$ vs. time (min) plot, and doubling times were then calculated using linear regression. Doubling times (mean ± S.D.): WT (strain PY79): 21.3 ± 2.6 min; FtsZ(T111A) (strain bAB270): 20.7 ± 2.7 min; FtsZ(D213A) (5 µM IPTG, strain bAB273): 20.2 ± 1.45 min; FtsZ(D213A) (10 µM IPTG, strain bAB273): 19.4 ± 2.1 min; FtsA overexpression (100 µM IPTG, strain bAB199): 21.0 ± 2.1 min; and MciZ overexpression (60 mM xylose, strain bAB274): 20.4 ± 1.9 min.

F Representative growth rate curves extracted from single cell time lapses. Doubling times (mean ± S.D.): wild type (strain PY79): 24.8 ± 1.4 min (n = 14); FtsZ(T111A) (strain bAB270): 22.3 ± 2.1 min (n = 29); FtsZ(D213A) (10 µM IPTG, strain bAB273, 10 µM IPTG): 24.3 ± 2.2 min (n = 18).

Supplemental Tables

Table S1: FDAA experimental conditions

Figure	Label 1	Label 2	Label 3
1A	1 mM HADA, 60 min	1 mM BADA, 5 min	2 mM TADA, 30 sec
1B-C	0.5 mM HADA, 90 min	2 mM BADA, 15 sec	2 mM TADA, 15 sec
1D	1 mM HADA, 60 min	2 mM TADA, 15-120 sec	
1E	0.5 mM HADA, 60 min	2 mM TADA, 15 sec	50 μg/mL Bocillin, 15 sec
4A	2 mM TADA, 3 min	2 mM HADA, 3 min	
4B, S6C: PC190723	1 mM HADA, 90 min	2 mM TADA, 1 min	
4B, S6C: Z(D213A)	1 mM HADA, 90 min	2 mM TADA, 1 min	
4B, S6C: MciZ	1 mM HADA, 90 min	2 mM TADA, 30 sec	
S1A	0.5 mM HADA, 90 min	2 mM TADA, 15 sec	2 mM BADA, 15 sec
S1B, 45s	1 mM HADA, 60 min	2 mM TADA, 45 sec	
S1B, 15s x3	1 mM HADA, 60 min	2 mM TADA, 15 sec x3	
S1C, left	1 mM HADA, 60 min	2 mM TADA, 30 sec	
S1C, center	0.5 mM TADA, 60 min	2 mM HADA, 30 sec	
S1C, right	1 mM HADA, 60 min	2 mM BADA, 30 sec	
S2D	1 mM HADA, 60 min	2 mM TADA, 2 min	
S2D (-Pbp2B)	1 mM HADA, 180 min	2 mM TADA, 2 min	
S6A	0.5 mM HADA, 90 min	1 mM TADA, 2 min	

Sample	Sample Size
Figure 1C and E	
Simultaneous	94
Sequential	103
Bocillin	101
Figure 1D, S2B-C	
15 sec	107
30 sec	98
45 sec	115
60 sec	94
90 sec	96
120 sec	108
Figure 4B, S6B-C	
– PC190723	103
+ PC190723	100
– FtsZ(D213A)	96
+ FtsZ(D213A)	92
– MciZ	92
+ MciZ	124
Figure S1B	
45s	100
15s x3	98
Figure S2D	
WT	73
Penicillin G	37
Vancomycin	48
Pbp2B depletion	33

Table S2: Strains and oligonucleotides used in this study

Strain Name	Genotype (all strains are PY79 unless otherwise noted)	Source
PY79	*Prototroph*	(*41*)
ME7	*pbp2B::mNeonGreen-15aa-pbp2B*	This Work
bGS3	*pbp2B::erm-Phyperspank-mNeonGreen-15aa-pbp2B*	This Work
bGS28	*pbp2B::erm-Phyperspank-HaloTag-15aa-pbp2B*	This Work
bGS31	*pbp2B::erm-Phyperspank-HaloTag-15aa-pbp2B, ftsZ::mNeonGreen-15aa-ftsZ*	This Work
bGS60	*pbp2B::erm-Phyperspank-HaloTag-15aa-pbp2B, ftsZΩftsZ(T111A) (tet)*	This Work
bGS90	*pbp2B::erm-Phyperspank-HaloTag-15aa-pbp2B, amyE::erm-Phyperspank-ftsAZ(D213A)*	This Work
AH93	*amyE::Pxyl-mciZ (cat)*	(*29*)
bAB94	*amyE::erm-Phyperspank-ftsA*	This Work
bAB96	*amyE::erm-Phyperspank-ftsZ*	This Work
bAB98	*amyE::erm-Phyperspank-ftsAZ*	This Work
bAB146	*amyE::erm-Phyperspank-mNeonGreen-15aa-pbp2B*	This Work
bAB167	*ftsA::ftsA-mNeonGreen(SW)*	This Work
bAB185	*ftsZ::mNeonGreen-15aa-ftsZ*	This Work
bAB199	*ftsZ::mNeonGreen-15aa-ftsZ, amyE::erm-Phyperspank-ftsA*	This Work
bAB209	*ftsZ::mNeonGreen-15aa-ftsZ, amyE::PxylA-mciZ (cat)*	This Work
bAB213	*ftsAZ::erm-ftsA-HaloTag(SW)-ftsZ-cat*	This Work
bAB215	*amyE::erm-Phyperspank-ftsAZ(D213A)*	This Work
bAB217	*amyE::erm-Phyperspank-ftsA-mNeonGreen(SW)-ftsZ(D213A)*	This Work
bAB219	*amyE::erm-Phyperspank-ftsA-mNeonGreen-15aa-ftsZ*	This Work
bAB221	*ftsZ::mNeonGreen-15aa-ftsZ, amyE::erm-Phyperspank-ftsA-mNeonGreen-15aa-ftsZ*	This Work
bAB229	*ftsAZ::erm-ftsA-HaloTag(SW)-mNeonGreen-15aa-ftsZ-cat*	This Work
bAB248	*ftsZ::mNeonGreen-15aa-ftsZ, amyE::Phyperspank-minCD (spc)*	This Work
bAB270	*pbp2B::mNeonGreen-15aa-pbp2B, ftsZΩftsZ(T111A) (tet)*	This Work
bAB271	*pbp2B::mNeonGreen-15aa-pbp2B, ftsZΩftsZ(G106S) (tet)*	This Work
bAB272	*pbp2B::mNeonGreen-15aa-pbp2B, amyE::erm-Phyperspank-ftsAZ*	This Work
bAB273	*pbp2B::mNeonGreen-15aa-pbp2B, amyE::erm-Phyperspank-ftsAZ(D213A)*	This Work
bAB274	*pbp2B::mNeonGreen-15aa-pbp2B, amyE::PxylA-mciZ (cat)*	This Work
AB62	*ftsZΩftsZ(T111A) (tet)*	(*42*)
bAB281	*amyE::erm-Phyperspank-ftsA-mNeonGreen-15aa-ftsZ, ftsZΩftsZ(T111A) (tet)*	This Work
bAB282	*amyE::erm-Phyperspank-ftsA-mNeonGreen-15aa-ftsZ, ftsZΩftsZ(G106S) (tet)*	This Work
bAB284	*pbp2B::mNeonGreen-15aa-pbp2B, amyE::Phyperspank-minCD (spc)*	This Work
bAB310	*pbp2B::mNeonGreen-15aa-pbp2B, amyE::erm-Phyperspank-ftsA*	This Work
168CA	*BS168CA trpC2*	(*43*)
PL642	JH642 – *ftsZ::ftsZ-gfp-cat*	(*44*)
SH13	168CA – *ftsZ:: ftsZ-GFP::cat*	This Work

PB5250	*Δhag::aph (Kan)*	(*45*)
SH33	168CA – *ftsZ:: ftsZ-GFP::cat, Δhag::aph (Kan)*	This Work
SH41	*ftsZ::mNeonGreen-15aa-ftsZ, Δhag::aph (Kan)*	This Work
Oligo Name	**Sequence (5' to 3')**	
oAB14	TGGCCTGAGCCCGGTCCCTGGCCAGATCCCTCGAGGCCGCTGATTTCTAAGGTAGAAAG	
oAB21	CTGGCCAGGGACCGGGCTCAGGCCAAGGAAGCGGCATGGCAGAAATCGGTACT	
oAB28	ATGCTATACGAACGGTAGTTGACCAGTGCTCCCTGGTTTCATGTCATTCAATT	
oAB29	ACATTATACGAACGGTACTGAGCGAGGGAGCAGAAGACAATATCTGTAATTCA	
oAB30	CCATCCTCATATGTCTGACC	
oAB33	TGGCCTGAGCCCGGTCCCTGGCCAGATCCCTCGAGGGCTTCGTCATAGTAGGC	
oAB44	TGACCAGATCCAGGACCTTGTCCGCTACCCTCAAGGCCGCTGATTTCTAAGGTAG	
oAB48	GCGGACAAGGTCCTGGATCTGGTCAAGGCAGTGGGTCGGAAGATGAAATATTTGA	
oAB74	TCACGAAAGCCATATCTTCC	
oAB75	AACGGTAGTTGACCAGTGCTCCCTGCATTTCATCATATGTACCTTG	
oAB76	GAACGGTACTGAGCGAGGGAGCAGAAGTATTTGTTTCCGGTTTCT	
oAB78	AGCGGATAACAATTAAGCTTTAAGGAGGAACTACCATGAACAACAATGAACTTTACGTC	
oAB81	GGCGAAAGAAGTCGTTAATG	
oAB82	AACGGTAGTTGACCAGTGCTCCCTGTCATTCCTGTATGTTTTTCACTTTTTTATC	
oAB87	GATCTTCATCGTGGCCCCGGGTTCATAC	
oAB93	CTTTCGGTAAGTCCCGTCTAGCCTTGCCCCTATTCCCAAAACATGCTTAATAGTTTTTTC	
oAB94	CTTTCGGTAAGTCCCGTCTAGCCTTGCCCTTAGCCGCGTTTATTACGGTTTC	
oAB113	GGTGTGGCTCTCATTGCTATAGGGGGAGGGTCAA	
oAB114	TTGACCCTCCCCCTATAGCAATGAGAGCCACACC	
oAB123	CAACCTTGACTTTGCTGCTGTGAAAACAATCATG	
oAB124	CATGATTGTTTTCACAGCAGCAAAGTCAAGGTTG	
oAB134	GGTAAGTCCCGTCTAGCCTTGCCCTTAATCAGGATTTTTAAACTTAACCTTGATTACGGT	
oAB135	CAGGGACCGGGCTCAGGCCAAGGAAGCGGCATGGTTTCGAAAGGAGAGGAGGATA	
oAB136	CCAGATCCAGGACCTTGTCCGCTACCCTCAAGCTTATAGAGTTCATCCATACCCATCACG	
oAB137	GGATAACAATTAAGCTTTAAGGAGGAACTACCATGGTTTCGAAAGGAGAGGAGGATA	
oAB139	TATCCTCCTCTCCTTTCGAAACCATGCTAAATCCTCCTAATCTGCCGAATG	
oAB140	GGACCGGGCTCAGGCCAAGGAAGCGGCATGTTGGAGTTCGAAACAAACATAGACG	
oJM28	CAGGGAGCACTGGTCAAC	
oJM29	TTCTGCTCCCTCGCTCAG	
oGS7	GGATAACAATTAAGCTTTAAGGAGGAACTACCATGGCAGAAATCGGTACTGG	
oMD191	TTTGGATGGATTCAGCCCGATTG	
oMD196	GGGCAAGGCTAGACGGG	
oMD197	TCACATACTCGTTTCCAAACGGATC	
oMD232	GGTAGTTCCTCCTTAAAGCTTAATTGTTATCCGCTCACAAT	
oME20	CTCGAGGGATCTGGCCAGGGACCGGGCTCAGGCCAAGGAAGCGGCATGATTCAAATGCCAAAA AAGAATAAATTTATGAATAGAG	
oME21	GAATTTGTGCAAATATTGATTGAGGCG	
oME22	CATAATTGTTTCTTCGCCTTTGCTGACCATTCATTCCTGTATGTTTTTCACTTTTTTATC	
oME32	AATAAATGTAGTGCGTAAGGAGGAACTCATATGGTCAGCAAAGGCGAAGAAAC	
oZB33	ATGGTTTCGAAAGGAGAGGAGGATAATATG	
oZB34	TGGCCTGAGCCCGGTCCCTGGCCAGATCCCTCGAGCTTATAGAGTTCATCCATACCCATC	
oZB46	ATGGTTTCGAAAGGAGAGGAGGATAATATGCAGGGAGCACTGGTCAACTACCGTTCGTAT	
oZB47	CATATTATCCTCCTCTCCTTTCGAAACCATATGAGTTCCTCCTTACGCACTACATTTATT	

Table S3: Live-cell imaging conditions

Figure	Imaging	Exposure Time 1	Intervals 1	Exposure Time 2	Intervals 2
2A	TIRF	1 sec (488 nm laser)	1 sec	-	-
2B	TIRF	1 sec (488 nm laser)	1 sec	-	-
2C	TIRF	500 msec (561 nm laser)	3 sec	500 msec (488 nm laser)	3 sec
2D	TIRF	1 sec (488 nm laser)	1 sec	-	-
2E	Near-TIRF	1 sec (488 nm laser)	1 sec	-	-
2F	TIRF	1 sec (561 nm laser)	1 sec	1 sec (488 nm laser)	snapshot
3A	TIRF	1 sec (488 nm laser)	1 sec	-	-
3B	TIRF	1 sec (488 nm laser)	1 sec	-	-
3C-left	TIRF	1 sec (488 nm laser)	1 sec	-	-
3C-right	TIRF	1 sec (561 nm laser)	1 sec	-	-
3D-left	TIRF	1 sec (488 nm laser)	1 sec	-	-
3D-right	TIRF	1 sec (561 nm laser)	1 sec	1 sec (488 nm laser)	snapshot
3E-left	TIRF	1 sec (488 nm laser)	1 sec	-	-
3E-right	TIRF	1 sec (561 nm laser)	1 sec	1 sec (488 nm laser)	snapshot
3F	TIRF	3 sec (488 nm laser)	3 sec	-	-
4A-top	Confocal	150 msec (488 nm laser)	30 sec	-	-
4C-top	Confocal	50-150 msec (488 nm laser)	1 min	-	-

Table S4: Measurements of FtsAZ filament velocities and Pbp2B ring constriction periods with different genetic perturbations, growth conditions and measurement methods

	FtsAZ Filament Velocity (nm/sec)		Constriction Time Kymographs (min)	
	Strain	**Average ± SD**	**Strain**	**Average ± SD**
Control	bAB185	32 ± 7.8 (n = 200)	ME7	10.2 ± 2.0 (n = 100)
FtsZ-G106S (Z84)	bAB282	28 ± 5.1 (n = 76)	bAB271	12.5 ± 3.5 (n = 100)
FtsZ-T111A	bAB281	21 ± 3.2 (n = 52)	bAB270	16.5 ± 2.1 (n = 100)
Up FtsAZ	bAB221	31 ± 5.8 (n = 200)	bAB272	9.4 ± 1.8 (n = 100)
Up FtsA	bAB199	20 ± 6.3 (n = 200)	bAB199	20.3 ± 4.0 (n = 100)
Up MciZ	bAB209	45 ± 9.0 (n = 200)	bAB274	7.0 ± 2.2 (n = 100)
Up MinCD	bAB248	35 ± 5.3 (n = 200)	bAB285	11.3 ± 1.9 (n = 100)
1μM FtsZ-D213A	bAB217	33 ± 7.5 (n = 200)	bAB273	10.0 ± 2.1 (n = 100)
5μM FtsZ-D213A	bAB217	23 ± 6.5 (n = 132)	bAB273	17.9 ± 3.0 (n = 100)
7.5μM FtsZ-D213A	bAB217	15 ± 3.8 (n = 133)	bAB273	21.2 ± 3.1 (n = 100)
10μM FtsZ-D213A	bAB217	13 ± 4.0 (n = 130)	bAB273	25.8 ± 9.9 (n = 100)
Pbp2B Depletion	bGS31	30 ± 5.4 (n = 200)	-	-
Penicillin G	bAB185	32 ± 5.3 (n = 200)	-	-

	Constriction Time Tracking (min)		Constriction Time Minimal Media at 25°C (min)	
	Strain	**Average ± SD**	**Strain**	**Average ± SD**
Control	ME7	9.5 ± 2.2 (n = 305)	ME7	30.9 ± 5.2 (n = 150)
FtsZ-T111A	bAB270	17.2 ± 4.8 (n = 239)	bAB270	49.9 ± 5.6 (n = 100)
Up MciZ	bAB274	7.4 ± 1.6 (n = 407)	bAB274	23.3 ± 5.7 (n = 100)
5μM FtsZ-D213A	bAB273	18.8 ± 5.2 (n = 119)	-	-
10μM FtsZ-D213A	-	-	bAB273	68.3 ± 16.6 (n = 65)

Movie captions

Movie S1: FtsA and FtsZ filaments move directionally together inside and outside of the division site. Cells were imaged using TIRF microscopy at 3 second intervals. Representative 5-minute acquisitions, displayed at 15 frames per second (45x actual speed). Scale bar: 2 μm.
Column 1: mNeonGreen-FtsZ (bAB185) showing filament motion.
Column 2: FtsA-mNeonGreen(SW) (bAB167) showing filament motion.
Column 3: FtsA-HaloTag(SW)-JF549 (red) and mNeonGreen-FtsZ (green) showing filament motion. bAB229 cells were incubated with 500 nM of HaloTag-JF549 ligand for 15 minutes.
Column 4: mNeonGreen-FtsZ (bAB221) showing filament motion with FtsAZ overexpressed. Cells were grown with 100 μM IPTG for 1 hour.

Movie S2: Imaging of vertically oriented cells in microholes shows FtsZ moves directionally in dense constricting Z rings.
mNeonGreen-FtsZ (strain SH41) dynamics in vertically immobilized cells with 600-1000 nm radii. Cells were imaged by epifluorescence at 1 second intervals. 2-minute acquisitions displayed at 15 frames per second (15x actual speed). Scale bar: 1 μm.

Movie S3: Pbp2B moves directionally around AZ rings
A. JF549-HaloTag-Pbp2B (bGS31) shows Pbp2B single molecules by TIRF microscopy. Cells were incubated with 50 pM of HaloTag-JF549 ligand for 15 minutes, washed, and prepared as indicated in methods. Cells were imaged at 1 second intervals using TIRF microscopy. Images of mNeonGreen-FtsZ were used to mark the position of the division machinery (first 60 frames of the movie) before imaging of JF549. Arrowheads indicate Z rings that colocalize with directionally moving Pbp2B. 4-minute acquisition displayed at 30 frames per second (30x actual speed).
B Overexpression of exogenous mNeonGreen-Pbp2B (100μM IPTG, bAB146) shows diffusion of Pbp2B molecules along the cell by TIRF microscopy. Cells were imaged at 100 millisecond intervals. 10-second acquisition displayed at 30 frame per second (3x actual speed). Scale bar: 2 μm.

Movie S4: FtsAZ filament motion is not stopped by inhibition of cell wall synthesis.
FtsA-mNeonGreen(SW) (bAB167) showing filament motion during perturbations to cell wall synthesis. Antibiotics were added to the top of the pad 5 minutes before imaging. Images shown as follows: no antibiotic control (top left); 50 mg/μl Vancomycin (top right); 10 mg/μl Ampicillin (center left); 10 mg/μl Penicillin G (center right); 100 mg/μl Cephalexin (bottom left) and 100 mg/μl Fosfomycin (bottom right). Cells were imaged at 1 second intervals with TIRF microscopy. Representative 5-minute acquisitions, displayed at 30 frames per second (30x actual speed). Scale bar: 2 μm.

Movie S5: FtsAZ filament motion is not dependent on Pbp2B.
A mNeonGreen-FtsZ (bAB185) shows absence of Z ring constriction following depletion of Pbp2B. Cells were grown to mid-exponential phase with 10 μM IPTG, inducer was washed out from medium and cells were imaged after 1 hour of growth without IPTG. Images were acquired at 30 second intervals for 1.5 hours using epifluorescence illumination. Movie displayed at 30 frames per second (900x actual speed).

B mNeonGreen-FtsZ (bAB185) continues to show FtsZ filament motion following depletion of Pbp2B. Cells were imaged with 2 hours of Pbp2B depletion (after no Z ring constriction was detected). Cells were imaged at 1 second intervals using TIRF microscopy. Representative 5-minute acquisitions, displayed at 30 frames per second (30x actual speed). Scale bars: 2 μm.

Movie S6: FtsAZ filament motion is driven by treadmilling.
A Low expression of mNeonGreen-FtsZ (bAB219) shows that single molecules of FtsZ are immobile at division sites. Cells were imaged at 500 millisecond intervals for 2 minutes by TIRF microscopy. Movie displayed at 30 frames per second (15x actual speed).
B Single molecules of FtsA-HaloTag(SW)-JF646 (bAB213) are immobile within division sites. Cells were imaged at 200 millisecond intervals for 1 minute using TIRF microscopy. Representative videos are displayed at 30 frames per second (6x actual speed). Scale bars: 2 μm.

Movie S7: FtsZ GTPase activity modulates FtsAZ filament treadmilling and directional motion.
A Inducible FtsA-mNeonGreen(SW)-FtsZ(D213A) (bAB217) titration showing motion of FtsA filaments in the presence of different induction levels of the GTPase-defective FtsZ(D213A). Cells were grown until mid-exponential phase, diluted and incubated 1 hour with 1 μM (top left), 5 μM (top right), 10 μM (bottom left) and 100 μM IPTG (bottom right). Cells were imaged at 3 second intervals for 5 minutes with TIRF microscopy. Movie displayed at 15 frames per second (45x actual speed).
B mNeonGreen-FtsZ (bAB185) showing motion of FtsZ filaments after the addition of MciZ peptide by perfusion in a CellAsic microfluidic chamber. Cells were imaged in CH medium (top left), then 10 minutes (top right) and 20 minutes (bottom left) after the addition of 1 μM MciZ. Sequentially, MciZ was washed out from cells for 10 minutes and cells were imaged again (bottom right). Cells were imaged at 3 second intervals for 5 minutes with TIRF microscopy. The exogenous addition (or expression) of MciZ causes two phases of effects on FtsZ dynamics: 1) Initially (between 0 and 10 minutes after exogenous addition or induction of MciZ), small FtsZ filaments move around the cell at a faster rate. During this period, all Z rings constricted faster than usual. At later time points (15-20 minutes), as the MciZ incubation time (or expression) increased, all FtsZ filaments and Z rings in the cell disappeared and did not return. Movie displayed at 15 frames per second (45x actual speed). Scale bars: 2 μm.

Movie S8: PC190723 blocks FtsAZ filament and Pbp2B directional motions.
A mNeonGreen-FtsZ (bAB185) showing motion of FtsZ filaments during treatment with PC190723, added by perfusion in a CellAsic microfluidic chamber. Cells were imaged at 3 second intervals in CH medium for 10 minutes, PC190723 (10 μM) was flowed over the cells, and cells were imaged for 10 minutes (top right). After this, PC190723 was washed out, and cells were imaged for 20 minutes. Movie displayed at 30 frames per second (90x actual speed).
B JF549-HaloTag-Pbp2B (bGS31) showing Pbp2B single molecules by TIRF microscopy during PC190723 treatment. Cells were incubated with 50 pM of HaloTag-JF549 ligand for 15 minutes prior to imaging. Cells were imaged 18 minutes after the addition of 3 μl of 10 mg/ml PC190723 on top of a 500 μl 2% agarose pad. Snapshot images of mNeonGreen-FtsZ were used to mark the position of the division machinery (first 60 frames of the movie, white arrowheads). Cells were imaged at 1 second intervals for 4 minutes with TIRF microscopy. Movie displayed at 30 frames per second (30x actual speed). Scale bars: 2 μm.

Movie S9: FtsAZ(D213A) overexpression creates slow-growing FtsAZ spirals.
FtsA-mNeonGreen(SW)-FtsZ(D213A) (bAB217) showing the growth of FtsA spirals by spinning-disk confocal microscopy. Cells were grown without inducer, placed under a 2% agarose CH pad containing 1 mM IPTG, and imaged at 30 second intervals for 2 hours. To make the transition from ring to spirals visible, histogram bleach correction was applied to all time lapses in Fiji to normalize signal between frames. Representative videos are displayed at 30 frames per second (900x actual speed). Scale bar: 2 μm.

Movie S10: FtsAZ filament velocity controls the rate of cytokinesis.
mNeonGreen-Pbp2B rings within cells of different genetic backgrounds were followed over time by confocal microscopy. Cells were imaged at 1 minute intervals for 2 hours. 6 examples out of 12 different conditions are shown as follows: wild type (top left), FtsAZ overexpression (top right), MciZ overexpression (center left), native FtsZ(T111A) mutant (center right), FtsZ(D213A) mutant expressed with 5 μM IPTG (bottom left), FtsZ(D213A) mutant expressed with 10 μM IPTG (bottom right). Representative 30-minute videos are displayed at 8 frames per second (480x actual speed). Scale bar: 2 μm.

References and Notes

1. Y. Chen, H. P. Erickson, Rapid in vitro assembly dynamics and subunit turnover of FtsZ demonstrated by fluorescence resonance energy transfer. *J. Biol. Chem.* **280**, 22549–22554 (2005). doi:10.1074/jbc.M500895200 Medline

2. P. Szwedziak, Q. Wang, T. A. M. Bharat, M. Tsim, J. Löwe, Architecture of the ring formed by the tubulin homologue FtsZ in bacterial cell division. *eLife* **3**, e04601 (2014). doi:10.7554/eLife.04601 Medline

3. X. Ma, D. W. Ehrhardt, W. Margolin, Colocalization of cell division proteins FtsZ and FtsA to cytoskeletal structures in living *Escherichia coli* cells by using green fluorescent protein. *Proc. Natl. Acad. Sci. U.S.A.* **93**, 12998–13003 (1996). doi:10.1073/pnas.93.23.12998 Medline

4. P. Gamba, J. W. Veening, N. J. Saunders, L. W. Hamoen, R. A. Daniel, Two-step assembly dynamics of the *Bacillus subtilis* divisome. *J. Bacteriol.* **191**, 4186–4194 (2009). doi:10.1128/JB.01758-08 Medline

5. E. Kuru, H. V. Hughes, P. J. Brown, E. Hall, S. Tekkam, F. Cava, M. A. de Pedro, Y. V. Brun, M. S. VanNieuwenhze, In situ probing of newly synthesized peptidoglycan in live bacteria with fluorescent D-amino acids. *Angew. Chem. Int. Ed. Engl.* **51**, 12519–12523 (2012). doi:10.1002/anie.201206749 Medline

6. T. J. Lupoli, H. Tsukamoto, E. H. Doud, T.-S. A. Wang, S. Walker, D. Kahne, Transpeptidase-mediated incorporation of D-amino acids into bacterial peptidoglycan. *J. Am. Chem. Soc.* **133**, 10748–10751 (2011). doi:10.1021/ja2040656 Medline

7. C. Eberhardt, L. Kuerschner, D. S. Weiss, Probing the catalytic activity of a cell division-specific transpeptidase in vivo with beta-lactams. *J. Bacteriol.* **185**, 3726–3734 (2003). doi:10.1128/JB.185.13.3726-3734.2003 Medline

8. S. Thanedar, W. Margolin, FtsZ exhibits rapid movement and oscillation waves in helix-like patterns in *Escherichia coli*. *Curr. Biol.* **14**, 1167–1173 (2004). doi:10.1016/j.cub.2004.06.048 Medline

9. V. W. Rowlett, W. Margolin, 3D-SIM super-resolution of FtsZ and its membrane tethers in *Escherichia coli* cells. *Biophys. J.* **107**, L17–L20 (2014). doi:10.1016/j.bpj.2014.08.024 Medline

10. C. Coltharp, J. Buss, T. M. Plumer, J. Xiao, Defining the rate-limiting processes of bacterial cytokinesis. *Proc. Natl. Acad. Sci. U.S.A.* **113**, E1044–E1053 (2016). doi:10.1073/pnas.1514296113 Medline

11. S. J. Holden, T. Pengo, K. L. Meibom, C. Fernandez Fernandez, J. Collier, S. Manley, High throughput 3D super-resolution microscopy reveals *Caulobacter crescentus* in vivo Z-ring organization. *Proc. Natl. Acad. Sci. U.S.A.* **111**, 4566–4571 (2014). doi:10.1073/pnas.1313368111 Medline

12. M. P. Strauss, A. T. F. Liew, L. Turnbull, C. B. Whitchurch, L. G. Monahan, E. J. Harry, 3D-SIM super resolution microscopy reveals a bead-like arrangement for FtsZ and the division machinery: Implications for triggering cytokinesis. *PLOS Biol.* **10**, e1001389 (2012). doi:10.1371/journal.pbio.1001389 Medline

13. D. E. Anderson, F. J. Gueiros-Filho, H. P. Erickson, Assembly dynamics of FtsZ rings in *Bacillus subtilis* and *Escherichia coli* and effects of FtsZ-regulating proteins. *J. Bacteriol.* **186**, 5775–5781 (2004). doi:10.1128/JB.186.17.5775-5781.2004 Medline

14. J. B. Grimm, B. P. English, J. Chen, J. P. Slaughter, Z. Zhang, A. Revyakin, R. Patel, J. J. Macklin, D. Normanno, R. H. Singer, T. Lionnet, L. D. Lavis, A general method to improve fluorophores for live-cell and single-molecule microscopy. *Nat. Methods* **12**, 244–250, 3, 250 (2015). doi:10.1038/nmeth.3256 Medline

15. E. C. Garner, R. Bernard, W. Wang, X. Zhuang, D. Z. Rudner, T. Mitchison, Coupled, circumferential motions of the cell wall synthesis machinery and MreB filaments in *B. subtilis*. *Science* **333**, 222–225 (2011). doi:10.1126/science.1203285 Medline

16. M. Loose, T. J. Mitchison, The bacterial cell division proteins FtsA and FtsZ self-organize into dynamic cytoskeletal patterns. *Nat. Cell Biol.* **16**, 38–46 (2014). doi:10.1038/ncb2885 Medline

17. L. Niu, J. Yu, Investigating intracellular dynamics of FtsZ cytoskeleton with photoactivation single-molecule tracking. *Biophys. J.* **95**, 2009–2016 (2008). doi:10.1529/biophysj.108.128751 Medline

18. S. D. Redick, J. Stricker, G. Briscoe, H. P. Erickson, Mutants of FtsZ targeting the protofilament interface: Effects on cell division and GTPase activity. *J. Bacteriol.* **187**, 2727–2736 (2005). doi:10.1128/JB.187.8.2727-2736.2005 Medline

19. D. J. Haydon, N. R. Stokes, R. Ure, G. Galbraith, J. M. Bennett, D. R. Brown, P. J. Baker, V. V. Barynin, D. W. Rice, S. E. Sedelnikova, J. R. Heal, J. M. Sheridan, S. T. Aiwale, P. K. Chauhan, A. Srivastava, A. Taneja, I. Collins, J. Errington, L. G. Czaplewski, An inhibitor of FtsZ with potent and selective anti-staphylococcal activity. *Science* **321**, 1673–1675 (2008). doi:10.1126/science.1159961 Medline

20. A. W. Bisson-Filho, K. F. Discola, P. Castellen, V. Blasios, A. Martins, M. L. Sforça, W. Garcia, A. C. M. Zeri, H. P. Erickson, A. Dessen, F. J. Gueiros-Filho, FtsZ filament capping by MciZ, a developmental regulator of bacterial division. *Proc. Natl. Acad. Sci. U.S.A.* **112**, E2130–E2138 (2015). doi:10.1073/pnas.1414242112 Medline

21. X. Yang *et al*., GTPase activity-coupled treadmilling of the bacterial tubulin FtsZ organizes septal cell-wall synthesis. *bioRxiv*, 10.1101/077610 (2016).

22. M. Osawa, H. P. Erickson, Liposome division by a simple bacterial division machinery. *Proc. Natl. Acad. Sci. U.S.A.* **110**, 11000–11004 (2013). doi:10.1073/pnas.1222254110 Medline

23. A. J. F. Egan, W. Vollmer, The stoichiometric divisome: A hypothesis. *Front. Microbiol.* **6**, 455 (2015). doi:10.3389/fmicb.2015.00455 Medline

24. Z. Li, M. J. Trimble, Y. V. Brun, G. J. Jensen, The structure of FtsZ filaments in vivo suggests a force-generating role in cell division. *EMBO J.* **26**, 4694–4708 (2007). doi:10.1038/sj.emboj.7601895 Medline

25. E. Kuru, S. Tekkam, E. Hall, Y. V. Brun, M. S. Van Nieuwenhze, Synthesis of fluorescent D-amino acids and their use for probing peptidoglycan synthesis and bacterial growth in situ. *Nat. Protoc.* **10**, 33–52 (2015). doi:10.1038/nprot.2014.197 Medline

26. H. C. Wang, R. C. Gayda, High-level expression of the FtsA protein inhibits cell septation in *Escherichia coli* K-12. *J. Bacteriol.* **172**, 4736–4740 (1990). doi:10.1128/jb.172.8.4736-4740.1990 Medline

27. S. J. Dewar, K. J. Begg, W. D. Donachie, Inhibition of cell division initiation by an imbalance in the ratio of FtsA to FtsZ. *J. Bacteriol.* **174**, 6314–6316 (1992). doi:10.1128/jb.174.19.6314-6316.1992 Medline

28. L. Araújo-Bazán, L. B. Ruiz-Avila, D. Andreu, S. Huecas, J. M. Andreu, Cytological profile of antibacterial FtsZ inhibitors and synthetic peptide MciZ. *Front. Microbiol.* **7**, 1558 (2016). doi:10.3389/fmicb.2016.01558 Medline

29. A. A. Handler, J. E. Lim, R. Losick, Peptide inhibitor of cytokinesis during sporulation in *Bacillus subtilis*. *Mol. Microbiol.* **68**, 588–599 (2008). doi:10.1111/j.1365-2958.2008.06173.x Medline

<jrn>30. J.-Y. Tinevez, N. Perry, J. Schindelin, G. M. Hoopes, G. D. Reynolds, E. Laplantine, S. Y. Bednarek, S. L. Shorte, K. W. Eliceiri, TrackMate: An open and extensible platform for single-particle tracking. *Methods* S1046-2023(16)30334-6 (2016). Medline</jrn>

31. F. Wu, B. G. C. van Schie, J. E. Keymer, C. Dekker, Symmetry and scale orient Min protein patterns in shaped bacterial sculptures. *Nat. Nanotechnol.* **10**, 719–726 (2015). doi:10.1038/nnano.2015.126 Medline

32. J. Männik, F. Wu, F. J. H. Hol, P. Bisicchia, D. J. Sherratt, J. E. Keymer, C. Dekker, Robustness and accuracy of cell division in *Escherichia coli* in diverse cell shapes. *Proc. Natl. Acad. Sci. U.S.A.* **109**, 6957–6962 (2012). doi:10.1073/pnas.1120854109 Medline

33. I. G. de Jong, K. Beilharz, O. P. Kuipers, J.-W. Veening, Live cell imaging of *Bacillus subtilis* and *Streptococcus pneumoniae* using automated time-lapse microscopy. *J. Vis. Exp.* **53**, e3145 (2011). Medline

34. J. Schindelin, I. Arganda-Carreras, E. Frise, V. Kaynig, M. Longair, T. Pietzsch, S. Preibisch, C. Rueden, S. Saalfeld, B. Schmid, J.-Y. Tinevez, D. J. White, V. Hartenstein, K. Eliceiri, P. Tomancak, A. Cardona, Fiji: An open-source platform for biological-image analysis. *Nat. Methods* **9**, 676–682 (2012). doi:10.1038/nmeth.2019 Medline

35. G. Ball, J. Demmerle, R. Kaufmann, I. Davis, I. M. Dobbie, L. Schermelleh, SIMcheck: A toolbox for successful super-resolution Structured Illumination Microscopy. *Sci. Rep.* **5**, 15915 (2015). doi:10.1038/srep15915 Medline

36. H. Hoffman, "violin. m-Simple violin plot using matlab default kernel density estimation" (INRES, University of Bonn, Katzenburgweg, 2015).

37. F. Zoergiebel, "PLOTERR" [general error bar plot] (MathWorks, Natick, MA, 2008).

38. F. O. Bendezú, C. A. Hale, T. G. Bernhardt, P. A. J. de Boer, RodZ (YfgA) is required for proper assembly of the MreB actin cytoskeleton and cell shape in *E. coli*. *EMBO J.* **28**, 193–204 (2009). doi:10.1038/emboj.2008.264 Medline

39. T. K. Lee, K. Meng, H. Shi, K. C. Huang, Single-molecule imaging reveals modulation of cell wall synthesis dynamics in live bacterial cells. *Nat. Commun.* **7**, 13170 (2016). doi:10.1038/ncomms13170 Medline

40. H. Cho, C. N. Wivagg, M. Kapoor, Z. Barry, P. D. A. Rohs, H. Suh, J. A. Marto, E. C. Garner, T. G. Bernhardt, Bacterial cell wall biogenesis is mediated by SEDS and PBP polymerase families functioning semi-autonomously. *Nat. Microbiol.* **1**, 16172 (2016). doi:10.1038/nmicrobiol.2016.172 Medline

41. P. J. Youngman, J. B. Perkins, R. Losick, Genetic transposition and insertional mutagenesis in *Bacillus subtilis* with *Streptococcus faecalis* transposon Tn917. *Proc. Natl. Acad. Sci. U.S.A.* **80**, 2305–2309 (1983). doi:10.1073/pnas.80.8.2305 Medline

42. V. Blasios, A. W. Bisson-Filho, P. Castellen, M. L. C. Nogueira, J. Bettini, R. V. Portugal, A. C. M. Zeri, F. J. Gueiros-Filho, Genetic and biochemical characterization of the MinC-FtsZ interaction in *Bacillus subtilis*. *PLOS ONE* **8**, e60690 (2013). doi:10.1371/journal.pone.0060690 Medline

43. F. Kunst, N. Ogasawara, I. Moszer, A. M. Albertini, G. Alloni, V. Azevedo, M. G. Bertero, P. Bessières, A. Bolotin, S. Borchert, R. Borriss, L. Boursier, A. Brans, M. Braun, S. C. Brignell, S. Bron, S. Brouillet, C. V. Bruschi, B. Caldwell, V. Capuano, N. M. Carter, S.-K. Choi, J. J. Cordani, I. F. Connerton, N. J. Cummings, R. A. Daniel, F. Denziot, K. M. Devine, A. Düsterhöft, S. D. Ehrlich, P. T. Emmerson, K. D. Entian, J. Errington, C. Fabret, E. Ferrari, D. Foulger, C. Fritz, M. Fujita, Y. Fujita, S. Fuma, A. Galizzi, N. Galleron, S.-Y. Ghim, P. Glaser, A. Goffeau, E. J. Golightly, G. Grandi, G. Guiseppi, B. J. Guy, K. Haga, J. Haiech, C. R. Harwood, A. Hènaut, H. Hilbert, S. Holsappel, S. Hosono, M.-F. Hullo, M. Itaya, L. Jones, B. Joris, D. Karamata, Y. Kasahara, M. Klaerr-Blanchard, C. Klein, Y. Kobayashi, P. Koetter, G. Koningstein, S. Krogh, M. Kumano, K. Kurita, A. Lapidus, S. Lardinois, J. Lauber, V. Lazarevic, S.-M. Lee, A. Levine, H. Liu, S. Masuda, C. Mauël, C. Médigue, N. Medina, R. P. Mellado, M. Mizuno, D. Moestl, S. Nakai, M. Noback, D. Noone, M. O'Reilly, K. Ogawa, A. Ogiwara, B. Oudega, S.-H. Park, V. Parro, T. M. Pohl, D. Portelle, S. Porwollik, A. M. Prescott, E. Presecan, P. Pujic, B. Purnelle, G. Rapoport, M. Rey, S. Reynolds, M. Rieger, C. Rivolta, E. Rocha, B. Roche, M. Rose, Y. Sadaie, T. Sato, E. Scanlan, S. Schleich, R. Schroeter, F. Scoffone, J. Sekiguchi, A. Sekowska, S. J. Seror, P. Serror, B.-S. Shin, B. Soldo, A. Sorokin, E. Tacconi, T. Takagi, H. Takahashi, K. Takemaru, M. Takeuchi, A. Tamakoshi, T. Tanaka, P. Terpstra, A. Togoni, V. Tosato, S. Uchiyama, M. Vandebol, F. Vannier, A. Vassarotti, A. Viari, R. Wambutt, H. Wedler, T. Weitzenegger, P. Winters, A. Wipat, H. Yamamoto, K. Yamane, K. Yasumoto, K. Yata, K. Yoshida, H. F. Yoshikawa, E. Zumstein, H. Yoshikawa, A. Danchin, The complete genome sequence of the gram-positive bacterium *Bacillus subtilis*. *Nature* **390**, 249–256 (1997). doi:10.1038/36786 Medline

44. P. A. Levin, I. G. Kurtser, A. D. Grossman, Identification and characterization of a negative regulator of FtsZ ring formation in *Bacillus subtilis*. *Proc. Natl. Acad. Sci. U.S.A.* **96**, 9642–9647 (1999). doi:10.1073/pnas.96.17.9642 Medline

45. S. Senesi, E. Ghelardi, F. Celandroni, S. Salvetti, E. Parisio, A. Galizzi, Surface-associated flagellum formation and swarming differentiation in *Bacillus subtilis* are controlled by the *ifm* locus. *J. Bacteriol.* **186**, 1158–1164 (2004). doi:10.1128/JB.186.4.1158-1164.2004 Medline